Regeneration following tissue necrosis is mediated by non-apoptotic caspase activity

Jacob W. Klemm, Chloe Van Hazel, Robin E. Harris

Arizona State University, 427 E Tyler Mall LSE 229, Tempe, AZ 85287-4501

Corresponding author: robin.harris@asu.edu

Running title: Dronc promotes necrosis-induced regeneration.

Abstract

Tissue necrosis is a devastating complication for many human diseases and injuries. Unfortunately, our understanding of necrosis and how it impacts surrounding healthy tissue – an essential consideration when developing methods to treat such injuries – has been limited by a lack of robust genetically tractable models. Our lab previously established a method to study necrosis-induced regeneration in the *Drosophila* wing imaginal disc, which revealed a unique phenomenon whereby cells at a distance from the injury upregulate caspase activity in a process called Necrosis-induced Apoptosis (NiA) that is vital for regeneration. Here we have further investigated this phenomenon, showing that NiA is predominantly associated with the highly regenerative pouch region of the disc, shaped by genetic factors present in the presumptive hinge. Furthermore, we find that a proportion of NiA fail to undergo apoptosis, instead surviving effector caspase activation to persist within the tissue and stimulate reparative proliferation late in regeneration. This proliferation relies on the initiator caspase Dronc, and occurs independent of JNK, ROS or mitogens associated with the previously characterized Apoptosis-induced Proliferation (AiP) mechanism. These data reveal a new means by which non-apoptotic Dronc signaling promotes regenerative proliferation in response to necrotic damage.

Introduction

Necrosis is the rapid, disordered death of cells characterized by the loss of membrane integrity and release of cytoplasmic contents into the surrounding tissue (Hajibabaie *et al.* 2023). This catastrophic type of cell death can occur in diverse tissues and is central to many human conditions, particularly those related to ischemic injuries. Such conditions can include chronic illnesses like diabetes, joint disorders, sickle-cell anemia and other inherited and congenital diseases (Masi *et al.* 2007, Mulay *et al.* 2016, Karsch-Bluman *et al.* 2019, Tonnus *et al.* 2021, Li *et al.* 2023), as well as more acute medical events like strokes, heart attacks, bacterial infections and common traumatic injuries (Konstantinidis *et al.* 2012, Hakkarainen *et al.* 2014, Bonne and Kadri 2017, Wu *et al.* 2018). Even therapeutic interventions, in particular treatments for cancer, can result in this devastating form of damage (Robertson *et al.* 2017, Nakada *et al.* 2019, Yang *et al.* 2021). Unfortunately, current strategies to treat necrosis mainly focus on invasive procedures that are often met with limited success. With such substantial bearings on human health, it is crucial to better understand the effects of necrosis in disease and injury, particularly in the context of tissue repair and regeneration.

Unfortunately, we currently have a limited understanding of how necrosis impacts surrounding healthy tissue during wound healing. Indeed, much of our understanding about how cell death influences tissue repair comes instead from models involving programmed cell death (PCD) like apoptosis (Hajibabaie *et al.* 2023). This highly regulated process can be triggered by intrinsic or extrinsic pathways, both of which lead to the activation of caspases that mediate the controlled disassembly of the cell (Ashkenazi and Salvesen 2014). Studies of PCD in a variety of species have shown that cells undergoing apoptosis can release signaling molecules that are interpreted by surrounding tissues to drive wound healing events, such as tissue remodeling, immune responses, survival and proliferation of surrounding cells (Tseng *et al.* 2007, Fan and Bergmann 2008, Chera *et al.* 2009, Bergmann and Steller 2010, Li *et al.* 2010, Pellettieri *et al.* 2010, Ryoo and Bergmann 2012, Vriz *et al.* 2014, Fuchs and Steller 2015, Perez-Garijo and Steller 2015, Fogarty and Bergmann 2017, Perez-Garijo 2018). For example, the signaling molecules Prostaglandin E2 and Hedgehog are produced by dying hepatocytes to induce regenerative proliferation in the vertebrate liver (Jung *et al.* 2010, Li *et al.* 2010), while apoptotic-deficient mice show both impaired liver regeneration and epidermal recovery after wounding (Li *et al.* 2010). While mitogenic signaling by apoptotic cells is an established and conserved process, whether similar signaling events occur following necrotic cell death is less clear.

Evidence of apoptotic signaling first originated from studies of the larval wing primordia in *Drosophila* (Perez-Garijo *et al.* 2004, Ryoo *et al.* 2004). This epithelial tissue has been extensively characterized as a model for growth, development and regeneration, including the role that cell death plays in these processes (Beira and Paro 2016, Worley and Hariharan 2022). Ongoing studies of this model have identified an essential signaling network centered on the highly conserved JNK pathway. JNK activates several major signaling

pathways including Hippo and JAK/STAT, which have conserved roles in promoting regeneration across species (Worley *et al.* 2012, Hariharan and Serras 2017, Fox *et al.* 2020, Worley and Hariharan 2022), as well as activating JNK itself via overlapping feed-forward loops. One such feed-forward mechanism acts through the initiator caspase Dronc (*Drosophila* Caspase-9), which, independent of its role in apoptosis, is translocated to the cell membrane to activate the release of ROS from the NADPH oxidase Duox (Amcheslavsky *et al.* 2018). ROS attracts hemocytes to further activate JNK signaling in the disc through the release of the TNF ligand Eiger (Fogarty *et al.* 2016, Diwanji and Bergmann 2018). In a related pathway, JNK can also lead to the expression of the *Duox* maturation factor *moladietz* (*mol*), thus activating this loop without Dronc (Khan *et al.* 2017, Pinal *et al.* 2018). An important advance in elucidating this network was the ability to generate “undead cells”, using the baculovirus caspase inhibitor P35 to prevent apoptotic cells from dying (Hay *et al.* 1994). These cells therefore persist, releasing mitogenic factors including Wingless (Wg, Wnt1), Decapentaplegic (Dpp, BMP2/4), Spitz (Spi, EGF) or Hedgehog (Hh) (Huh *et al.* 2004, Perez-Garijo *et al.* 2004, Ryoo *et al.* 2004, Perez-Garijo *et al.* 2005, Fan and Bergmann 2008, Perez-Garijo *et al.* 2009, Morata *et al.* 2011, Fan *et al.* 2014). These signals subsequently promote proliferation of the surrounding cells in a phenomenon known as Apoptosis-induced Proliferation (AiP) (Fan and Bergmann 2008, Ryoo and Bergmann 2012, Fogarty and Bergmann 2017).

By contrast, the genetic events following necrosis are less well explored. Necrosis is characterized by swelling and loss of cellular membrane integrity, with the release of cellular contents into the intercellular space causing a significant inflammatory response (Festjens *et al.* 2006, D'Arcy 2019, Hajibabaie *et al.* 2023). Necrosis is highly variable, occurring as a regulated process, for example necroptosis, or as unregulated, caspase-independent cell lysis (Ashkenazi and Salvesen 2014, D'Arcy 2019). The factors released from necrotic cells are collectively termed Damage-Associated Molecular Patterns (DAMPs)(Venereau *et al.* 2015, Roh and Sohn 2018), which are thought to interact with pattern recognition receptors (PRRs) on nearby cells, mostly of the Toll-like receptor (TLR) family (Ming *et al.* 2014, Gong *et al.* 2020). DAMPs are understood to mainly consist of fundamental cellular components like histones, chromatin, and actin (Venereau *et al.* 2015, Gordon *et al.* 2018, Roh and Sohn 2018), although specific factors have been also been described. For example, High-mobility group box 1 (HMBG1) has been characterized as a DAMP in models of spinal cord, cardiac and muscle injury where it promotes angiogenesis, attracts repair cells and induces proliferation (Venereau *et al.* 2015), as well as in *Drosophila* models of necrosis (Nishida *et al.* 2024). However, the overall role of DAMPs and how they influence healing and regeneration through interaction with healthy tissues has yet to be fully explored.

To investigate necrosis-induced wound repair and regeneration, our lab developed a method to rapidly and reproducibly induce necrotic cell death within the developing *Drosophila* wing imaginal discs (Klemm *et al.* 2021). Using a genetic ablation system we previously established, named Duration and Location (DUAL) Control (Harris 2023), we can induce necrosis in the wing disc via expression of a leaky cation channel

GluR1^{LC} (Liu *et al.* 2013, Yang *et al.* 2013). Using this system (*DC*^{GluR1}), we showed that wing discs are capable of fully regenerating following necrotic injury at a level comparable to that of damage induced by apoptosis (Klemm *et al.* 2021). However, while apoptotic ablation leads to JNK signaling and extensive caspase activity, we found that necrosis leads to only a minor level of JNK-mediated apoptosis, which is confined to the wound edge, but unexpectedly generates significant caspase activity in cells distant from the injury. We called this non-autonomous caspase activation Necrosis-induced Apoptosis (NiA) (Klemm *et al.* 2021). Unlike normal apoptotic cells, NiA form entirely independent of JNK signaling, and cannot be made undead using P35. We also demonstrated that NiA is essential for regeneration, although how was unclear.

Here we have further characterized the NiA phenomenon, finding that only regeneration-competent areas of the wing disc can produce NiA following damage, in part due to WNT and JAK/STAT signaling in the hinge that limits NiA to the pouch. Building upon our finding that NiA is necessary for regeneration, we show that NiA leads to localized proliferation significantly later in regeneration than previously appreciated. Using tools to trace caspase activity and cell death, we demonstrate that this is possible because a proportion of NiA survive effector caspase activation and persist late into regeneration where they promote proliferation. Finally, we show that this proliferation relies on the initiator caspase Dronc, but surprisingly does not involve established AiP mechanisms. Our data suggest a model in which necrotic injuries induce caspase activity in cells at a distance from the injury, some of which undergo JNK-independent apoptosis (NiA), while others survive and promote proliferation through a novel non-apoptotic function of Dronc, which is separate from its role in AiP. We refer to these surviving NiA cells as Necrosis-induced Caspase-Positive (NiCP) cells. These findings reveal an important genetic response to lytic cell death that could potentially be leveraged to augment regeneration of necrotic wounds.

Results

Formation of NiA occurs primarily in the wing pouch.

Previously, we found that NiA occurs in the lateral pouch (LP) upon induction of necrosis in the distal pouch with *DC*^{GluR1} (Figure 1A, D and E, yellow arrowheads in E) (Klemm *et al.* 2021). The wing disc itself comprises different identities reflecting the adult structures they ultimately create, including the pouch, hinge and notum, which are themselves divided into compartments; anterior/posterior and dorsal/ventral (Figure 1B). Since these various disc identities have distinct regenerative capacities stemming from their different genetic responses to damage (Martin *et al.* 2017), to better understand the formation of NiA and the role it plays in regeneration, we tested whether necrosis occurring in different areas of the disc leads to NiA. To do so, we utilized *GAL4/UAS/GAL80*^{ts} to conditionally express *UAS-GluR1*^{LC} in the pouch, hinge or notum tissues (Figure 1B and C) (Yang *et al.* 2013). As an initial test, we attempted to recapitulate our original observations made using *DC*^{GluR1} by employing an enhancer of the *spalt* gene driving *GAL4*

(*R85E08^{ts}>GluR1*) to cause necrosis in the distal pouch (Figure 1F and G). As anticipated, NiA are formed in the LP following 20 hr of ablation (denoted as 0 hr, when larvae are downshifted to 18°C) (Figure 1G). In this figure and others, NiA are recognized as cells positive for the cleaved caspase Dcp-1 and negative for GFP that labels the ablation domain (*UAS-GFP*) (Figure 1E and G, yellow arrowheads), which indicates that these caspase-positive cells originate outside the area of ablation. This test confirms that the NiA phenomenon occurs independent of the ablation system used. Notably, NiA are consistently absent from the presumptive hinge region surrounding the pouch following both *R85E08^{ts}>GluR1* or *DC^{GluR1}* ablation (Figure 1E and G). Indeed, outside of the pouch, Dcp-1 is only observed in a small area of the posterior pleura (Figure 1E, red arrowhead) and at low levels stochastically across the disc resulting from temperature changes (Klemm *et al.* 2021). To further investigate the extent to which necrotic pouch tissue can induce NiA we next ablated the entire pouch using *rotund-GAL4* (*rn^{ts}>GluR1*) or *nubbin-GAL4* (*nub^{ts}>GluR1*) (Figure 1H, I and J, figure 1- figure supplement 1A). Necrosis of the whole pouch with either driver results in significant Dcp-1 (Figure 1I and Figure 1 – figure supplement 1A). However, the majority of these cells also have GFP and frequently overlap with expression of the JNK target *Mmp1* (Figure 1I and J), therefore resembling cells undergoing JNK-mediate apoptosis, such as those at the wound edge (WE) following distal pouch ablation (Figure 1 – figure supplement 1B, arrowhead), rather than NiA (Klemm *et al.* 2021)). These data suggest that cells outside of the pouch are generally unable to respond to DAMPs released by pouch cells undergoing necrosis to generate NiA, or that such DAMPs are spatially limited.

To test whether necrosis in areas outside of the pouch can induce NiA, we ablated the proximal notum using *pannier-GAL4* (*pnr^{ts}>GluR1*) (Figure 1K), using the absence of the notum Wg stripe to confirm loss of this area (Figure 1L and M, open arrowheads). We observed only minimal NiA, with sporadic Dcp-1-positive, GFP-negative cells in the unablated areas of the notum (Figure 1L), which remains unchanged after 24 hr (Figure 1M). To test the hinge, we used a putative *zfh1* enhancer driving *GAL4* (*R73G07^{ts}>GluR1*), which has hinge-specific expression (Figure 1N). Ablation of the hinge fails to generate NiA in the notum, but surprisingly does not induce a response in the neighboring pouch cells (Figure 1O and P, open arrowhead in O), despite their demonstrated ability to form NiA (Figure 1G). Together, these data suggest that only the pouch releases DAMPs - and has the requisite PRRs to respond to these DAMPs - that lead to NiA following necrosis.

As the efficacy of DAMPs might be limited by how far they can reach after being released from lysed cells, we also induced necrosis in the entire posterior disc compartment with *hedgehog-GAL4* (*hh^{ts}>GluR1*) (Figure 1Q), and in an anterior stripe along the anterior/posterior compartment boundary using *patched-GAL4* (*ptc^{ts}>GluR1*) (Figure 1 – figure supplement 1C). These experiments cause the simultaneous necrosis of pouch, hinge and notum tissues, allowing us to determine the potential of these different tissue identities to produce NiA. In both experiments, NiA cells are observed in the pouch, and to a lesser extent the notum, but are still strikingly absent from the hinge (Figure 1R, R' and T, Figure 1 – figure supplement 1D, D' and

F). After 24 hr of recovery, there is an increase in the number of NiA within the pouch and notum, but not the hinge (Figure 1S, S' and T, Figure 1 – figure supplement 1E, E' and F). Thus, it appears that NiA can occur outside of the pouch when a large enough area, or an area that also includes the pouch, is ablated. However, the hinge is refractory to NiA formation.

To avoid any bias in the use of tissue-specific *GAL4* drivers, we also made RFP-labeled stochastic clones that have the potential to undergo necrosis upon changing the growth temperature to 30°C (Figure 1 – figure supplement 1G). After allowing these clones to develop, we triggered necrosis in early third larval instar and examined the extent of active caspase in the different disc regions (Figure 1 – figure supplement 1H). As expected, necrosis of clones in the pouch leads to active caspases both within and surrounding the ablated area, including cells without the RFP clone label, suggesting that NiA has occurred (Figure 1 – figure supplement 1H', arrowheads). We also found that necrosis in the notum leads to comparatively little caspase labeling (Figure 1 – figure supplement 1H'') consistent with the notum being less able to generate NiA. Necrotic clones in the hinge also produces caspase activity, but most of these cells also have RFP, suggesting again that NiA does not occur in the hinge (Figure 1 – figure supplement 1H'). Notably, the use of clones that naturally vary in size also demonstrates that the area of ablation is related to the amount of NiA produced (Figure 1 – figure supplement 1I), a trend also seen with the tissue-specific ablation experiments (Figure 1 – figure supplement 1I).

Together, these data infer three important conclusions: 1) all areas of the disc can be killed by necrosis and therefore potentially can release DAMPs, 2) NiA is limited to the pouch when local necrosis occurs, but when multiple (or large) areas of the disc are killed, limited NiA can also be induced in the notum, although we cannot rule out that this is due to DAMPs from dying pouch cells, and 3) the hinge is refractory to NiA, which is consistent with other findings that show its resistance to apoptosis in response to irradiation (Verghese and Su 2016). Thus, the overall pattern of competence to undergo NiA appears to reflect the uneven regenerative capacity of the wing disc, with NiA formation predominantly associated with the highly regenerative wing pouch.

NiA is regulated by WNT and JAK/STAT signaling.

As NiA readily occurs in the pouch but is excluded from the nearby hinge, we used this contrasting response to identify genetic factors that might regulate NiA formation. The wing hinge is specified by JAK/STAT signaling during disc development, which can protect cells from irradiation-induced apoptosis potentially via the expression of *Zn finger homeodomain* 2 (*zfh2*) (La Fortezza *et al.* 2016, Verghese and Su 2016, Verghese and Su 2018). Alongside JAK/STAT, the presence of Wingless (Wg, *Drosophila* Wnt1), which encircles the pouch, may also protect cells from death and permit regeneration of the pouch through the

repression of *reaper* (*rpr*) (Verghese and Su 2016). As such, we investigated both JAK/STAT and Wg to determine whether they regulate NiA formation.

The activity of the JAK/STAT pathway can be visualized in the hinge of early third instar larval discs by a *10XSTAT-GFP* reporter (Bach *et al.* 2007)(Figure 2A). Upon ablation of the distal pouch with DC^{GluR1}, a high level of JAK/STAT activity is observed at the immediate WE (Figure 2B, arrowhead), similar to its upregulation following irradiation or apoptotic ablation (Herrera and Bach 2019). As JNK signaling is induced at the WE (Figure 1 – figure supplement 1B) (Klemm *et al.* 2021), and the *unpaired* ligands are targets of JNK signaling (Katsuyama *et al.* 2015, Jaiswal *et al.* 2023), this JAK/STAT activity is likely to be JNK-mediated. By contrast, much lower levels of JAK/STAT activity are observed in the areas of the pouch where NiA occurs (Figure 2B, open arrowheads), surrounded by the higher developmental JAK/STAT in the hinge (Figure 2B). To determine if low JAK/STAT activity is important for NiA, we knocked down the receptor *domeless* ($UAS\text{-}dome^{RNAi}$) in the pouch, which results in a significant increase in NiA (Figure 2C, D and E), suggesting that JAK/STAT signaling may negatively regulate the formation of NiA. To further test this idea, we ectopically activated JAK/STAT (*UAS-hop48A*). However, even in the absence of damage, this expression results in high levels of caspase positive cells (Figure 2 – figure supplement 1A and B), making it difficult to determine an effect on NiA formation. Therefore, to further investigate if JAK/STAT regulates NiA formation, we asked whether reducing developmental JAK/STAT in the hinge might lead to NiA spreading further into this region. We generated a version of DUAL Control that expresses *GAL4* in the posterior compartment by replacing the pouch-specific *DVE>>GAL4* with *hh-GAL4* (Figure 2F and G, Figure 2 – figure supplement 1C). To prevent *hh-GAL4* from being active throughout development, we included $GAL80^{ts}$ (hereafter $DC^{GluR1}hh^{ts}$) and used temperature changes to limit *GAL4* activity to the period just prior to ablation (Figure 2F). With this system, we knocked down the expression of the JAK/STAT transcription factor *Stat92E* ($UAS\text{-}Stat92E^{RNAi}$) in the posterior compartment and ablated the distal pouch, which again shows an increase in caspase-positive cells in the pouch (Figure 2I, arrowhead), but surprisingly NiA cells are still not observed in the hinge (Figure 2I, open arrowhead). To confirm this result, we also targeted *zinc finger homeodomain 2* (*Zfh2*), a downstream target of the JAK/STAT pathway that potentially protects cells from apoptosis (La Fortezza *et al.* 2016, Verghese and Su 2018). The knockdown of *Zfh2* also does not result in any hinge-specific NiA formation, although an increase in pouch NiA was again observed (Figure 2 – figure supplement 1E). Knockdown of *Stat92E* or *Zfh2* under non-ablating conditions does not yield any increase in caspase signal (Figure 2H, Figure 2 – figure supplement 1D). Thus, JAK/STAT signaling appear to limit NiA formation in the pouch, while the inability for NiA to expand into the hinge upon reducing JAK/STAT suggests that other hinge-specific factors may be involved.

Wg has also been shown to protect cells from apoptosis in the hinge (Verghese and Su 2016), and therefore could influence the formation of NiA. Unlike the stochastic heat shock-induced apoptosis (Figure 2J), we noted that NiA in the pouch frequently occurs in discrete populations that avoid Wg at the margin stripe and

the inner Wg circle at the boundary of the pouch and hinge (Figure 2K), limiting formation of the NiA cells to regions that appear to overlap the *vestigial quadrant enhancer* (*vgQE-lacZ*, Figure 2 – figure supplement 1F and G) (Kim *et al.* 1996). By contrast, Dcp-1-positive cells at the WE do not avoid the Wg margin stripe (Figure 2K, arrowhead), suggesting that this behavior may be specific to NiA. To test this, we utilized $DC^{GluR1}hh^{ts}$ to knock down *wg* in the posterior compartment of the disc ($UAS\text{-}wg^{RNAi}$) and found that NiA now occurs in areas of the pouch where *wg* expression is lost, including the wing margin and inner hinge (Figure 2M, arrowhead), unlike NiA in the anterior (Figure 2M, open arrowhead). The increase in Dcp-1-positive cells does not occur when *wg* signaling is similarly blocked without damage (Figure 2L). Notably, the converse experiment in which *wg* is ectopically expressed during ablation does not suppress NiA (Figure 2 – figure supplement 1H and I), consistent with our hypothesis that other factors, such as targets downstream of JAK/STAT, might act alongside Wg to regulate NiA. Together, these data demonstrate that both WNT and JAK/STAT signaling act to limit NiA, thus potentially constraining it to the pouch following necrosis.

NiA promotes proliferation late in regeneration.

As NiA is spatially regulated by at least two major signaling pathways in the disc, we next focused on how the localization of NiA relates to its role in promoting regeneration. In our previous work, using an E2F reporter (*PCNA-GFP*) we found that the appearance of NiA coincides with an uptick in proliferation at 18 hr post-ablation close to the wound, which persists at 24 hr post ablation (Klemm *et al.* 2021). However, our investigation at subsequent time points of recovery shows that regenerative proliferation continues to increase through 36 hr and 48 hr of regeneration, later than initially assayed (Figure 3A-A'''). To quantify this proliferation, we used EdU to assay the relative level of cell proliferation in discs throughout regeneration from 18 hr to 48 hr post-ablation with DC^{GluR1} (Figure 3B-B'''), using folds as landmarks to normalize EdU intensity in the pouch relative to the disc (Figure 3 – figure supplement 1A-A'''). We also performed the same time course with apoptotic ablation using DC^{hepCA} for comparison (Figure 3C-C'''). At 18 hr of regeneration following ablation with either DC^{GluR1} or DC^{hepCA}, cells at the WE have already migrated distally to close the injury, while EdU is absent from an area immediately adjacent to the wound (Figure 3B and C). This is consistent with the recently described JNK-mediated pause in proliferation that occurs in regenerating wing discs (Jaiswal *et al.* 2023). At 24 hr, this proliferation-devoid area continues to persist following apoptotic injury (DC^{hepCA}) and the EdU signal becomes elevated broadly across the rest of the pouch, representing the formation of a blastema (Figure 3C'). By contrast, at 24 hr after necrosis (DC^{GluR1}), the EdU label is reestablished in cells around the wound showing that proliferation has restarted in these cells (Figure 3B'). Unlike DC^{hepCA}, the rest of the pouch does not appear to change its rate of proliferation (Figure 3B'). By 36 hr following necrosis, an intense uptick in EdU occurs broadly across the pouch, which is significantly stronger compared to discs ablated by apoptosis (Figure 3B'', C'' and E). This increase is maintained at 48 hr and remains consistently higher in DC^{GluR1} versus DC^{hepCA} ablated discs (Figure 3B''', C''' and E). Thus,

the timeline of recovery from necrosis appears to be distinct from that of apoptotic injury, with the strongest increases in regenerative proliferation occurring at comparatively later stages.

These observed increases in proliferation at 36 hr occur after the appearance of NiA. We previously showed that blocking the apoptotic pathway by simultaneously knocking down DIAP1 inhibitors *rpr*, *hid* and *grim* (*UAS-mir(RHG),* (Siegrist *et al.* 2010) throughout the pouch limits the initial uptick in proliferation at early stages (18 – 24 hr) and inhibits regeneration (Klemm *et al.* 2021). However, it remains unclear whether this newly observed late increase in regenerative proliferation (at 36 hr and 48 hr) also relies on a functional apoptotic pathway, and moreover, to what extent this regenerative proliferation relies on the JNK-mediated apoptosis at the WE versus the JNK-independent NiA in the LP. To answer these questions, we blocked apoptosis throughout the pouch and this time examined proliferation in late regeneration using EdU (Figure 3D-D'''). We found that the significant increase in EdU signaling at 36 hr is lost (Figure 3D'' and F), although by 48 hr this increase is mostly restored (Figure 3D''' and F). Importantly, the expression of *mir(RHG)* does not influence EdU levels in the absence of damage (Figure 3 – figure supplement 1B, C and D). Together, these data confirm that a functional apoptotic pathway is necessary to induce increases in proliferation late in regeneration following necrosis. To understand the relative contribution of WE apoptosis or the NiA in the LP, we designed experiments to block apoptosis in each disc area alone (*LP>mir(RHG),* Figure 3I, and *WE>mir(RHG)*, Figure 3J, see Materials and Methods for genotypes) relative to the whole pouch knock down (Figure 3G vs H). Strikingly, the high levels of EdU normally present at 36 hr are strongly reduced when apoptosis is blocked in either population (Figure 3K-O), suggesting that dying cells at the WE and the NiA in the LP both contribute to regenerative proliferation following necrosis. These data agree with our previous findings that the overall ability to regenerate adult wings is dependent on both populations (Klemm *et al.* 2021).

NiA does not promote proliferation through Apoptosis-induced Proliferation (AiP).

The question remains as to how NiA promotes regenerative proliferation. In *Drosophila*, cells undergoing apoptosis secrete factors such as Wg and Dpp to induce the proliferation of neighboring cells as part of a JNK-dependent Apoptosis-induced Proliferation (AiP) (Fogarty and Bergmann 2017). Although NiA occurs independent of JNK, to determine whether NiA-induced proliferation relies on any of the same signaling factors as AiP, we examined the damage-specific expression of these various secreted factors. To ensure we could visualize such signals, we used *lacZ*-based reporters and generated undead cells by expressing the baculoviral P35 (*UAS-P35*) in the whole pouch. This protein inhibits activity of the effector caspases Drice and Dcp-1 to block cell death (Hay *et al.* 1994), thus allowing signals produced by these cells to be readily detected. Following ablation with DC^{GluR1}, ectopic *wg* and *dpp* expression (*wg-lacZ* and *dpp-lacZ*) is observed at the WE (Figure 4C and C' vs A-B', and Figure 4F and F' vs D-E', arrowheads in C' and F')

coinciding with JNK activity in this region (Klemm *et al.* 2021). However, *lacZ* is not observed in the LP where NiA occurs (Figure 4C' and F', open arrowheads), indicating that these cells do not activate these mitogens. Similarly, we did not see expression of the EGF ligand *spitz* (*spi-lacZ)* in DC^{GluR1} ablated discs (Figure 4 – figure supplement 1A and B), which is observed during AiP in the eye (Fan *et al.* 2014). These results suggest that NiA does not promote proliferation through the same signaling factors as those seen during AiP.

We also tested whether other elements required for AiP are involved in NiA-induced proliferation. In addition to mitogen production, AiP also involves the production of extracellular reactive oxygen species (ROS) through a non-apoptotic function of Dronc that activates Duox. (Fogarty *et al.* 2016, Fogarty and Bergmann 2017, Amcheslavsky *et al.* 2018, Diwanji and Bergmann 2018). We first examined the extent of ROS production using dihydroethidium (DHE). This assay showed high levels of ROS localized to the WE but not in the LP (Figure 4G, arrowhead), suggesting that NiA does not produce ROS during regeneration. Consistent with this finding, the removal of ROS through pouch-wide expression of either the ROS chelators *Catalase* and *Superoxide dismutase 1* (*UAS-Cat; UAS-Sod1*) or knockdown of *Duox* ($UAS\text{-}Duox^{RNAi}$) has no observable effect on the appearance of NiA (Figure 4H and I), although apoptosis at the WE is strongly suppressed in both experiments (Figure 4H and I, open arrowhead). It has also been shown that the Duox maturation factor *moladietz* (*mol*) is upregulated following injury to sustain the production of ROS (Khan *et al.* 2017, Pinal *et al.* 2018). However, while a minor increase in the expression of a *mol* reporter (*mol-lacZ*) occurs at the WE (Figure 4 – figure supplement 1C and D, arrowhead in D), no change in *lacZ* is observed in response to necrosis in the LP. Finally, to functionally test whether AiP is required for the proliferation associated with NiA, we examined EdU levels across the disc at 36 hr when P35 is expressed. Normally, when undead cells are created via P35, ectopic mitogen production results in increased proliferation and tumorous overgrowth. However, when P35 is expressed solely in the LP we saw no change in EdU labeling versus controls (Figure 4J, L and M), suggesting NiA do not form undead cells. When expressed in the whole pouch, P35 has a small but non-significant effect on EdU (Figure 4J, K and M), consistent with undead cells now being generated at the WE. Together, these data indicate that cells at the WE undergo AiP to contribute to regenerative proliferation, while NiA promote proliferation through a different mechanism.

A subset of cells undergoing NiA are both caspase-positive and have markers of DNA repair and proliferation.

Robust populations of NiA appear in the wing pouch at around 18 hr of regeneration, (Figure 3 and (Klemm *et al.* 2021), while a strong increase in EdU labeling that encompasses much of the damaged pouch is detected later in regeneration at 36 hr and 48 hr (Figure 3B'', E and F). Since the loss of NiA abolishes this

change in proliferation (Figure 3M and O), we sought to understand how NiA might be influencing proliferation at these later time points. To do so, we used a highly sensitive sensor for the activity of the effector caspases Dcp-1 and Drice, *Green Caspase-3 Activity indicator* (*UAS-GC3Ai*, (Schott *et al.* 2017) to label NiA throughout regeneration (Figure 5A-E). With this reporter we found that, unlike normal apoptotic cells that are rapidly cleared from the wing disc (Figure 5J'), NiA persist at 36 hr when proliferation strengthens (Figure 5C), as well as at 48 hr (Figure 5D), and even up to 64 hr (wandering stage (Figure 5E), when regeneration is complete and pouch tissue is restored (Figure 5E, arrowhead). These persistent *GC3Ai*-positve cells are also frequently associated with cells actively undergoing mitosis by 36 hr, indicated by PH3 labelling (Figure 5F). Since the position of NiA cells change over time from 18 hr when they first appear to 36 hr when the uptick in proliferation occurs, to confirm that these GC3Ai-positive cells originally derive from NiA in the LP rather than the WE, we restricted *GC3Ai* expression to this part of the pouch (*LP>GC3Ai*, Figure 5G and H). The *GC3Ai* construct is tagged with an HA epitope that can be used to show its expression even in the absence of activation by caspases (Figure 5 – figure supplement 1A and B), which we used to confirm that its expression is limited to the LP (Figure 5G and H, Figure 5 – figure supplement 1C). With this experimental setup, we found that *GC3Ai*-positive cells are still present throughout the pouch at 36 hr (Figure 5G open arrowhead versus 5H arrowhead), confirming that the source of persistent caspase-positive cells is indeed NiA rather than the WE.

As NiA cells appear to be maintained in the disc for an extended period, we wondered how their behavior and morphology compared to that of normal apoptotic cells. When apoptosis is induced in wing discs using DC^{hepCA}, GC3Ai labeling shows apoptotic cells present in the pouch at 18 hr (Figure 5I) throughout the disc proper (Figure 5I'). At 36 hr these cells appear pyknotic and are basally extruded by 64 hr (Figure 5J-J'). By comparison, upon ablation with DC^{GluR1}, caspase-positive cells are seen to occupy different regions of the disc at 18 hr, with WE apoptotic cells closer towards the basal surface and NiA derived from the LP still within the disc proper (Figure 5K and K'). By 36 hr, the NiA form two distinct populations, some that are rounded up and appear closer to the basal surface, similar to the WE cells (Figure 5L and L' red arrowhead in L'), and others that continue to exhibit a columnar appearance and contact both the apical and basal surfaces of the disc (Figure 5L and L', yellow arrowheads in L'). The appearance and position of these cells suggest that a proportion of NiA cells may fail to complete apoptosis but instead persist into late stages of regeneration, despite the presence of detectible caspase activity. This is supported by the observation that only a minority of GC3Ai-positive cells have blebbing and pyknotic nuclei (Figure 5F', red arrowhead), while the majority appear to have a consistent and undisturbed cytoplasmic fluorescent label (Figure 5F', yellow arrowhead). To test our hypothesis that these cells are not undergoing apoptosis, we performed a TUNEL assay to fluorescently label cells with double stranded DNA breaks in GC3Ai-expressing discs. We found that most GC3Ai-labeled cells are co-labeled by TUNEL in early (18 hr) and late (36 hr) stages of regeneration (Figure 5 – figure supplement 1D and E). However, while TUNEL is associated with apoptosis,

by itself it does not confirm that cells are dying (Grasl-Kraupp *et al.* 1995). Therefore, we also examined levels of γH2Av, a histone variant associated with DNA repair and inhibition of apoptosis following damaging stimuli such as irradiation (Madigan *et al.* 2002). Interestingly, we found that GC3Ai-positive cells initially have high levels of γH2Av at 18 hr of regeneration, including those at the WE and the NiA (Figure 5 – figure supplement 1F, arrowheads), which is later lost from the NiA at 36 hr (Figure 5 – figure supplement 1G, open arrowheads). This indicates that NiA are undergoing active DNA repair rather than apoptosis. Taken together, these data suggest that a majority of NiA may upregulate caspase activity, but rather than undergoing apoptosis, they repair cellular damage and persist in the tissue into late stages of regeneration where they promote proliferation. As such, we are distinguishing this population of persistent and potentially non-apoptotic NiA by referring to them as Necrosis-induced Caspase Positive (NiCP) cells.

NiCP cells have initiator caspase activity but sublethal effector caspase activity.

The question remains as to why some cells (NiA) undergo apoptosis and are removed from the tissue in response to necrosis, while others (NiCP) persist despite caspase activity. The ability for cells to survive caspase activity is not surprising, as many non-apoptotic roles for caspases have been documented (Su 2020), including promoting proliferation. As mentioned, the initiator caspase Dronc functions in a non-apoptotic role to activate Duox and thus promote proliferation during AiP in damaged wing discs (Fogarty *et al.* 2016). Therefore, we wondered whether the difference between NiA and NiCP might arise from the level or activity of caspases within these cells. The GC3Ai reporter indicates activity of Dcp-1 and Drice (Schott *et al.* 2017) while the anti-cleaved-Dcp-1 antibody is thought to also detect Drice (Li *et al.* 2019). Thus, these tools exclusively detect effector caspases. To gain a better understanding of caspase activity in NiCP we used two additional methods: the Drice-Based Sensor *(DBS-GFP*), which provides a readout for activity of the initiator caspase Dronc (Baena-Lopez *et al.* 2018), and CasExpress, a *GAL4*-based tool that provides a readout for the activity of both effector caspases Drice and Dcp-1 (Ding *et al.* 2016), but unlike the other effector caspase monitoring tools we have used, its sensitivity can be modulated via $GAL80^{ts}$ (Colon Plaza and Su 2024). Our results show a strong overlap of *DBS-GFP* with anti-Dcp-1 in the LP of DC^{GluR1} ablated discs (Figure 6A and A'), indicating that these cells have robust Dronc activity, as do the cells at the WE (Figure 6A and A'). However, when we used CasExpress to examine effector caspase activity with a protocol that eliminates background developmental caspase activity (Colon Plaza and Su 2024), we noted that only cells at the WE were labelled (Figure 6B, B' and B'', arrowhead in B''), most of which had pyknotic nuclei showing they are actively undergoing apoptosis, while few cells in the LP were labelled (Figure 6B'', open arrowhead). We hypothesized that the level of effector caspase activity might be high enough to be detected by GC3Ai and the Dcp-1 antibody, but not by CasExpress. To further test this idea, we attempted to detect NiCP with CasExpress by combining it with GTRACE (Evans *et al.* 2009), which should lineage trace cells that have effector caspase activity, permanently labeling them with GFP at the start of ablation.

Again, we found that only cells of the WE are labelled during regeneration (Figure 6B''', arrowhead), with minimal labelling of cells in the LP (Figure 6B''', open arrowhead), even after 36 hr of regeneration when the NiCP-induced uptick in proliferation occurs (Figure 6 – figure supplement 1A). By comparison, performing these same experiments using *DC*^{hepCA} to induce extensive apoptotic cell death leads to a significant proportion of Dcp-1-positive cells being labelled by CasExpress under both normal and lineage tracing conditions despite their ongoing elimination (Figure 6C, arrowheads), suggesting that in the context of necrosis there is not enough effector caspase activity to label NiCP using these methods. Indeed, if the CasExpress experiment is performed in the absence of the *GAL80*^{ts} that suppresses the background developmental caspase signal, the NiCP cells now become labeled by GFP (Figure 6D), indicating that effector caspases are indeed present in these cells, but at potentially low enough levels to avoid death. Evidence for the existence of a cellular execution threshold of caspase activity in cells of the wing disc, which must be reached to induce apoptosis, has previously been documented (Florentin and Arama 2012). This is further supported by the observation that the GFP label becomes more apparent later in regeneration (Figure 6E), confirming that cells with effector caspase activity persist rather than die. Thus, it appears that in response to necrosis, the cells of the LP activate the initiator caspase Dronc and the effector caspase(s) Drice/Dcp-1 (to an extent) but fail to undergo programmed cell death. Instead, these cells persist in the disc late into regeneration where they stimulate regenerative proliferation.

Dronc in NiCP cells promote proliferation independent of AiP.

While NiCP cells have both initiator (Dronc) and effector caspase (Drice/Dcp-1) activity, it appears that the level or function of effector caspases is insufficient to cause apoptosis, and is also inconsequential for promoting regeneration – indeed, blocking Drice/Dcp-1 activity with P35 does not affect the increase in regenerative proliferation observed at 36 hr (Figure 4L and M), or the overall ability to regenerate (Klemm *et al.* 2021). This is in contrast with the ability of effector caspases to drive proliferation in the eye disc (Fan and Bergmann 2008). However, blocking the apoptotic pathway upstream of Dronc using *mir(RHG)* eliminates NiA/NiCP (Figure 7A, C and K, (Klemm *et al.* 2021), blocks the increase in proliferation (Figure 7B, D and L), and limits regeneration (Klemm *et al.* 2021). These observations demonstrate that proliferation induced by NiCP must depend on factors downstream of Rpr/Hid/Grim and upstream of the effector caspases Drice/Dcp-1, thus potentially pointing to a role for Dronc. To test this, we ablated discs with *DC*^{GluR1} while reducing the activity of Dronc using a null allele (*Dronc*^{I29}*/+,* (Xu *et al.* 2005)). With this genetic background there is a significant reduction in regenerative proliferation at 36 hr (Figure 7F and L, open arrowhead in F) and regeneration is limited, shown by both adult wing scores (Figure 7M) and wing size (Figure 7 – figure supplement 1A). These data demonstrate an essential role for Dronc in NiCP to promote proliferation and subsequent regeneration of the disc following necrosis. We noted that this mutant does not strongly affect the appearance of Dcp-1 (Figure 7E and K), likely because this allele does not completely

suppress apoptosis, and thus the Dcp-1 label, unless homozygous (Xu *et al.* 2005), which is precluded by the genetics of this experiment. As an alternative, we interfered with Dronc function by expressing a dominant negative form of *Dronc* that contains only the caspase recruitment (CARD) pro-domain, here referred to as *Dronc*^{DN}, which blocks activation of Dcp-1/Drice and apoptosis (Meier *et al.* 2000). *Dronc*^{DN} reduces NiCP number, but to a lesser degree than *mi(RHG)* (Figure 7G and K) and does not affect proliferation (Figure 7H and L), suggesting that the CARD domain is dispensable for NiCP-induced proliferation.

Finally, we wondered how this might relate to the previously documented role of Dronc in promoting proliferation following apoptotic cell death during AiP (Fogarty and Bergmann 2017). AiP depends on both JNK and ROS (Fogarty *et al.* 2016), which we have shown are only present at the WE and are not associated with NiA/NiCP (Figure 4G, H and I). Thus, it is possible that Dronc's function in response to necrosis occurs via a distinct mechanism. Importantly, the activity of Dronc in both apoptosis and in AiP is influenced by Dronc's upstream regulator, DIAP1 (Meier *et al.* 2000). DIAP1 modifies Dronc's CARD domain to block both apoptosis (Kamber Kaya *et al.* 2017), and AiP (Fan and Bergmann 2008, Fogarty and Bergmann 2017). Thus, we expressed *DIAP1* (*UAS-DIAP1*) following ablation with *DC*^{GluR1} and found that it strongly suppresses the number of Dcp-1-positive cells at the WE and the NiA/NiCP in the LP (Figure 7I and K, open arrowheads in I), but strikingly has no effect on regenerative proliferation at 36 hr (Figure 7J and L). These results demonstrate a key role for the initiator caspase Dronc in promoting regenerative proliferation following necrosis, which is not affected by DIAP1, and therefore is likely separate from its role in apoptosis and the AiP mechanism.

Taken together, our data suggest a model in which necrosis leads to the establishment of distinct cell populations important for regeneration (Figure 7N). After injury, cells at the immediate WE undergo JNK-mediated apoptosis and contribute to proliferation via the established AiP mechanism (Figure 7N). while cells at a distance from the injury in the LP activate Dronc via an unknown DAMP-like signal(s) that occurs independent of JNK. Some of these cells go on to activate effector caspases at levels high enough to result in apoptosis (NiA, Figure 7N), while others activate these caspases at a low enough level to be detectable but insufficient to induce death (NiCP, Figure 7N). Instead, these cells persist in the tissue late into the repair process, where they promote proliferation via a novel non-apoptotic and AiP-independent function of the initiator caspase Dronc.

Discussion

An important and often overlooked factor when studying regeneration is the type of injury, and consequently the type of cell death it causes, which significantly impacts the repair processes. The existence of conserved signaling events that promote recovery has been well established in the context of apoptosis (Fogarty and Bergmann 2017, Perez-Garijo 2018), while the importance of such events in necrosis are less understood. Here, we have investigated the genetic events that occur in the aftermath of necrosis and how they influence the ability of a tissue to recover and regenerate. We previously showed that wing discs can regenerate effectively in the face of necrotic cell death (Klemm *et al.* 2021), triggering local JNK-dependent AiP at the WE, which is likely in response to tissue disruption (La Marca and Richardson 2020), while also inducing caspase activity in cells at a distance from the wound. This induction is independent of JNK signaling and, alongside having effector caspase activity, these cells can be marked by TUNEL and be blocked by inhibiting the apoptotic pathway (Klemm *et al.* 2021). As such, we determined that these cells are undergoing PCD and named this phenomenon Necrosis-induced Apoptosis (NiA). We also showed that both NiA and AiP at the wound contribute to regeneration. Our current work further characterizes the NiA phenomenon, and we have now shown that cells undergoing NiA in fact comprise two populations with separate behaviors. Upon necrosis, cells of the LP appear to activate effector caspases, indicated by cleaved Dcp-1 antibody staining and activation of the transgenic reporter GC3Ai. While a proportion of these cells develop apoptotic morphology, round up and are cleared over time as part of NiA, a large number of cells appear able to persist despite the presence of caspases, where they promote regenerative proliferation dependent on the initiator caspase Dronc (Figure 7N). To reflect these new findings, we have called these Necrosis-induced Caspase Positive (NiCP) cells. As these events occur in the absence of JNK, and exhibit none of the established hallmarks of AiP, including the presence and requirement for ROS, the ability to be blocked by DIAP1, or the production of mitogens such as Wg and Dpp, our results have identified an new function of Dronc in promoting regeneration in response to necrotic cell death.

The signal from necrotic cells that leads to NiA/NiCP is unknown.

Although we have shown that necrosis leads to NiCP cells and NiA at a distance from the site of injury, the signal that leads to these events is still unknown. Cells undergoing necrosis release DAMPs, a category of molecules that includes both common cellular contents as well as specific proteins, both of which can produce downstream responses like inflammation and the activation of effectors that promote a healing response (Gordon *et al.* 2018). DAMPs of both categories have been demonstrated in *Drosophila*; in apoptosis-deficient larvae, circulating DAMPs in the hemolymph can constitutively activate immune signaling in the fat body (Nishida *et al.* 2024), while specific factors such as α-actinin (Gordon *et al.* 2018), and HMGB1 (Nishida *et al.* 2024) are known to possess DAMP activity. Recent work describing an *in vivo* sensor for HMGB1 demonstrates the release of this DAMP from wing disc cells in response to a necrotic stimulus

similar to that used here (Nishida *et al.* 2024), making this an important candidate to test for a potential role in producing NiCP. However, it is equally possible that the causative DAMP(s) is one or more of the common fundamental cellular components released upon cell lysis, which would be more challenging to test. Considering the potential diversity and variable nature of DAMPs, it may be more feasible to instead identify the downstream PRRs that are required to interpret this unknown signal. Several groups of genes can act as PRRs, most notably the Toll-like receptor (TLR) family, various members of which can respond to DAMPs (Ming *et al.* 2014, Gong *et al.* 2020). Nine TLR genes have been identified in *Drosophila*, which have assorted roles in development and innate immunity (Anthoney *et al.* 2018), and have been implicated in DAMP sensing (Ming *et al.* 2014). Thus, it would be valuable to test the requirement for TLRs, alongside other suspected PRRs such as scavenger receptors (Cao 2016, Roh and Sohn 2018, Gong *et al.* 2020) for their requirement to induce NiCP.

An additional approach to elucidating how these cells are generated is by leveraging our finding that both JAK/STAT and WNT signaling seem to block NiCP/NiA in the disc. JAK/STAT signaling promotes survival of cells in response to stress by repressing JNK signaling, thus minimizing JNK-mediated apoptosis (La Fortezza *et al.* 2016). Although NiCP appear to avoid damage-induced JAK/STAT upregulation in the pouch, it is unlikely that this mechanism is responsible, since NiCP cells occur independent of JNK activity (Klemm *et al.* 2021). However, within the hinge, which is completely devoid of NiCP, JAK/STAT protects cells from apoptosis potentially by upregulating *DIAP1* (Verghese and Su 2016) and *zfh2* (Verghese and Su 2018), while Wg represses the transcription of *rpr*, (Verghese and Su 2016). Both signaling pathways are required autonomously in hinge cells for their ability to replace and regenerate ablated pouch tissue (Verghese and Su 2016, Ledru *et al.* 2022). Our results show that DIAP1 can prevent Dcp-1 activation in NiCP in the pouch, but not the corresponding proliferation that they produce, suggesting one reason that NiCP is not seen in the hinge is possibly due to the high DIAP1 threshold, which blocks Dronc's ability to activate effector caspases in this region. This may be in addition to a role for the JAK/STAT target *Zfh2*, which negatively regulates NiCP in the pouch. Thus, it remains to be seen whether lowering DIAP1 levels in the hinge, or manipulating Wg to allow *rpr* expression alongside changes in JAK/STAT and/or *zfh2*, might alter the appearance of NiCP in this region. Finally, the observation that both NiCP cells and their associated proliferative effects appear to occur independent of JNK signaling, which is normally central in models of stress and damage (Pinal *et al.* 2019), could help to narrow the identity of upstream signaling factors that leads to NiCP following necrosis. Together, these approaches could provide essential information as to the underlying genetic and cellular events that connect the lysis of cells during necrosis to the formation of NiCP cells required for regeneration.

The persistence of NiCP cells versus their elimination via NiA.

Our work shows that cells in the LP can either persist as NiCP and contribute to regenerative proliferation, or progress to apoptosis as part of NiA, but how this decision is made is unknown. During apoptosis in the wing disc, a threshold level of effector caspases must be reached for the cell to complete PCD (Florentin and

Arama 2012). Thus, we hypothesize that DAMP signals from necrotic cells may result in inconstant levels of effector caspase activity in cells of the LP – some with high caspases that advance to apoptosis (NiA), recognized by the changes in morphology and position in the disc characteristic of PCD, and others (NiCP cells) that have low enough caspase activity levels to survive, but this activity can still be detected by sensitized reagents. This is supported by our observations made using effector caspase-based lineage tracing using CasExpress (Ding *et al.* 2016), in which caspases can only be detected in NiCP cells by lowering the detection threshold. Alternatively, since CasExpress is a membrane-based reporter (Ding *et al.* 2016), it is also possible that effector caspases within NiCP cells have a different subcellular localization that reflects a non-apoptotic function, thus preventing reporter activation, rather than a difference in expression level or activity. The idea that caspases have different functions, both apoptotic and non-apoptotic, based on localization is well established, such as the targeting of specific cleavage substrates in distinct subcellular compartments (Brown-Suedel and Bouchier-Hayes 2020), or the trafficking of Dronc to the membrane to promote ROS (Amcheslavsky *et al.* 2018). Whatever the mechanism is that distinguishes between elimination via NiA or persistence as NiCP, the proportion of LP cells that participate in each remains difficult to assay due to the dynamic nature of cell death (Nano and Montell 2024) and overall variability of the NiCP/NiA phenotype. Anecdotal evidence from our experiments examining GC3Ai-labelled cells over time suggests that most cells in fact do not undergo apoptosis and are therefore NiCP. However, the use of other tools with potentially different sensitivities to effector caspases, such as Apoliner (Bardet *et al.* 2008), or CD8-PARP-Venus (Florentin and Arama 2012), may shed further light on this issue. Nevertheless, it remains to be seen how a cell becomes NiCP or undergoes NiA and dies, and whether distinct levels of caspases (initiator or effector), their localization, or a different attribute is responsible.

How does NiCP contribute to regeneration?

One of the most important questions that must be addressed is how the phenomena we have identified lead to regeneration following necrosis. Our experiments suggest that different caspase-positive populations of cells may contribute to regenerative proliferation: Firstly, the smaller number of apoptotic cells at the WE that likely contribute by the established process of JNK-dependent AiP (Fogarty and Bergmann 2017). Secondly, the caspase-surviving NiCP cells in the LP that contribute via an unknown process requiring the initiator caspase Dronc. Crucially, this non-apoptotic function of Dronc cannot be inhibited by the expression of DIAP1, which has previously been shown able to block both the apoptotic and non-apoptotic AiP functions of Dronc (Meier *et al.* 2000). Thus, our results suggest that Dronc acts in a different mechanism to induce growth in response to necrosis. The current understanding of how Dronc functions at the molecular level may provide valuable clues as to how. DIAP1 suppresses Dronc through its E3 ubiquitin ligase activity, which mono-ubiquitylates the CARD domain of Dronc to suppress both apoptotic and non-apoptotic functions related to AiP (Meier *et al.* 2000). Here, we find that the ectopic expression of *DIAP1* or just the

CARD-containing pro-domain of Dronc (*Dronc*^{DN}) cannot block regenerative proliferation while, by contrast, heterozygosity for the *Dronc*^{I29} null allele that can inhibit AiP (Kamber Kaya *et al.* 2017), is sufficient to block NiCP-mediated proliferation. Thus, regulation of Dronc activity in the context of necrosis may not rely on the modification of its CARD domain. Dronc's documented functions can also require its catalytic domain; mutations in this domain block the activation of Drice, and AiP-induced overgrowth (Fan *et al.* 2014). Thus, it will be important to assay whether the catalytic domain of Dronc is necessary to induce regenerative proliferation via NiCP. Similarly, although the CARD and catalytic domains are important points of regulation for Dronc activity, it has also been shown that damage-specific context cues are also vital. For example, the ectopic expression of *Dronc*^{K78R}, a mutant that cannot be repressed by DIAP1, might be expected to induce significant apoptotic cell death. However, this is not the case unless its structural binding partner, the APAF1 ortholog encoded by *Dark*, is expressed alongside (Shapiro *et al.* 2008), demonstrating the importance of stoichiometry between Dronc and Dark for the apoptotic function of Dronc. As such, further investigation into Dronc's functional domains and context-dependent interactions with its binding partners, including DIAP1 and Dark, will likely be necessary to understand how Dronc is involved in promoting regenerative proliferation in response to necrotic injury.

NiCP as a general mechanism to promote regeneration

Although initially characterized for their central role in apoptosis, many non-apoptotic functions of caspases have since been discovered, showing them to be dynamic regulators of diverse processes including cell fate specification, cellular remodeling, tissue growth, development, metabolism and others (Shinoda *et al.* 2019, Wang and Baker 2019, Su 2020). Studies of caspase signaling during regeneration have revealed essential non-apoptotic activities, such as initiator and effector-dependent models of AiP that contribute to repair (Ryoo and Bergmann 2012, Fogarty and Bergmann 2017). The contrasts in caspase functions that we have observed between apoptotic and necrotic damage, despite ultimately resulting in comparable levels of regeneration (Klemm *et al.* 2021), underscores the nuance that exists in damage signaling between different injury contexts. It is clear that caspase activity in response to injury as a mechanism to promote regeneration is a highly conserved process that occurs in many organisms, regardless of tissue identify or type of damage incurred (Bergmann and Steller 2010, Vriz *et al.* 2014, Fuchs and Steller 2015, Perez-Garijo and Steller 2015, Fogarty and Bergmann 2017, Perez-Garijo 2018). Our findings reinforce the position that we still have much to learn about the role of caspases in tissue repair, and that the type of injury, and thus the nature of cell death involved, is a vital consideration when developing effective wound-healing strategies.

Materials and Methods

Drosophila stocks

Flies were cultured in conventional dextrose fly media at 25°C with 12h light–dark cycles. The recipe for dextrose media contains 9.3 g agar, 32 g yeast, 61 g cornmeal, 129 g dextrose, and 14 g tegosept in 1 L distilled water. Genotypes for each figure panel are listed in the Supplementary Genotypes file. Fly lines used as ablation stocks are as follows: hs-FLP; hs-p65; salm-LexADBD, DVE>>GAL4 (DC^{NA}), hs-FLP; hs-p65; salm-LexADBD/ TM6C, sb (DC^{NA} no GAL4), hs-FLP; lexAop-GluR1^{LC}, hs-p65/ CyO; salm-LexADBD, DVE>>GAL4/ TM6B, Tb (DC^{GluR1}), hs-FLP; lexAop-GluR1^{LC}, hs-p65/CyO; salm-LexADBD/TM6C, sb (DC^{GluR1} no GAL4), hs-FLP;lexAOp-GluR1^{LC}/ CyO; salm-LexADBD, hh-GAL4/ TM6B, Tb (DC^{GluR1} hh-GAL4), hs-FLP;lexAop-hepCA, hs-p65/CyO; salm-DBD, DVE>>GAL4/ TM6B, Tb (DC^{hepCA}), UAS-GluR1; tubGAL80^{ts}, and tubGAL80^{ts}. The stock DR^{WNT}-GAL80 was used to limit *UAS*- transgenes to the lateral pouch (LP) where NiA occur (Klemm *et al.* 2021), while *R85E08-GAL4* was used to drive *UAS*- expression at the wound edge (WE). The following stocks were obtained from Bloomington Drosophila Stock Center: UAS-y^{RNAi} (BL#64527), UAS-p35 (BL#5073), UAS-hepCA (BL#58981), UAS-GC3Ai (II, BL#84346), UAS-GC3Ai (III, BL#84343), rn-GAL4 (BL#7405), hh-GAL4 (BL#600186), ptc-GAL4 (BL#2017), pnr-GAL4 (BL#), (BL#25758), nub-GAL4 (BL#25754), R73G07-GAL4(BL#39829), UAS-Zfh2RNAi (BL#50643), UAS-wg^{RNAi} (BL#32994), UAS-Stat92ERNAi (BL#35600), UAS-TCF^{DN} (II, BL#4784), dpp-lacZ (BL#8412), wg-lacZ (BL#50763), spi-lacZ (BL#10462), UAS-p35 (II, BL#5072), UAS-p35 (III, BL#5073), AP-1-GFP (Chatterjee and Bohmann 2012), act>>GAL4, UAS-RFP (BL#30558), DBS-GFP (III, BL#83130), DBS-QF (BL#83131), QUAS-FLP, act>>lacZ (BL#83133), CasExpress (BL#65419), G-trace (III, BL#28281), tubGAL80^{ts} (II, BL#7019), tubGAL80^{ts} (III, BL#7017), 10xSTAT-GFP (BL#), UAS-dome^{RNAi} (BL#32860), UAS-hop48A (BL#), PCNA-GFP (BL#25749), UAS-Cat (BL#24621), UAS-Sod1 (BL#24754), UAS-Duox^{RNAi} (BL#32903), mol-lacZ (BL#12173), rpr-lacZ (BL#98451), UAS-rpr^{RNAi} (BL#51849), UAS-dronc^{RNAi} (BL#32963), UAS-Dronc^{DN} (BL#58992), UAS-Strica^{RNAi}, UAS-DIAP1 (BL#6657), UAS-Dcp-1^{RNAi} (BL#38315), UAS-Drice^{RNAi} (BL#32403), and dronc^{I29}/TM3, Sb (BL#98453). UAS-mir(RHG) was gifted from the Hariharan lab at UC Berkeley. vgQE-lacZ was gifted from Tin Tin Su. UAS-GluR1^{LC} (Liu *et al.* 2013) was gifted from the Xie lab at Stowers Institute.

Ablation experiments

DUAL Control ablation with *DVE>>GAL4*. DUAL Control experiments were performed essentially as described in Harris et al. (2020). Briefly, experimental crosses were cultured at 25°C and density controlled at 50 larvae per vial. Larvae were heat shocked on 3.5 of development (84 hr after egg deposition (AED)) by placing vials in a 37°C water bath for 45 min, followed by a return to 25°C. Larvae were allowed to recover for 18 hr before being dissected, fixed and immunolabeled, unless otherwise indicated. *UAS-y^{RNAi}* and *UAS-*

GFP were used as control lines for RNAi-based experiments. w^{1118} was used as a control for *Dronc*^{I29} experiments. *DVE>>GAL4* drives expression in the wing pouch, allowing for the regenerating wound edge cells and NiA cells to be targeted for interrogation (Klemm *et al.* 2021). The *DR*^{WNT}*-GAL80* transgene (Klemm *et al.* 2021) was included as necessary to restrict *UAS*- expression to the LP where NiA/NiCP occurs.

DUAL Control ablation without *DVE>>GAL4*. To restrict *UAS*- expression to WE apoptotic cells, a version of DUAL Control lacking the DVE>>GAL4 (*DC*^{GluR1} *no GAL4*) was crossed to the *R85E08-GAL4* driver. *DC*^{GluR1}*no GAL4* experiments were performed along the same parameters as *DC*^{GluR1} experiments.

DUAL Control ablation with *hh-GAL4*. DUAL Control flies bearing *hh-GAL4* (*DC*^{GluR1}*hh*^{ts}) were cultured at 18°C and density controlled at 50 larvae per vial. *tubGAL80*^{ts} was included to conditionally express *UAS*-based constructs after ablation. Larvae were heat-shocked on day 7 of development (168 hr AED) for 45 min at 37°C, followed by incubation at 30°C to inactivate *tubGAL80*^{ts} and permit *UAS*-based expression. Larvae were allowed to recover for 18 hr before being dissected, fixed, and immunolabeled.

***GAL4/UAS* ablation.** *GAL4/UAS*-based ablation experiments were performed essentially as described in Smith-Bolton et al. (2009). Briefly, larvae bearing *UAS-GluR1; tubGAL80*^{ts} were cultured at 18°C and density controlled at 50 larvae per vial. Larvae upshifted on day 7 of development (168 hr AED) for 20 hr at 30°C and were either immediately dissected (denoted as 0 hr) or were allowed to recover for 24 hr before being dissected, fixed, and imaged. *tubGAL80*^{ts} flies were used as a non-ablating control.

***FLP*/FRT ablation experiments.** To generate clonal patches of *UAS-GluR1; UAS-RFP*-expressing cells, flies of the genotype *hs-FLP; AP-1-GFP; act>>GAL4, UAS-RFP/ T(2:3)SM6A, TM6B, Tb* were crossed to flies bearing *UAS-GluR1; tubGAL80*^{ts}. Larvae were cultured at 18°C and heat shocked in a 37°C water bath for 10 min at 42 hr AEL, returned to 18°C, and upshifted to 30°C for 18 hr at 168 h AEL, followed by dissection and immunostaining. *tubGAL80*^{ts} flies were used as a non-ablating control.

Regeneration scoring and wing measurements.

Adult wings were scored and measured after genotype blinding by another researcher. Scoring was performed on anesthetized adults by binning into a regeneration scoring category (Harris *et al.* 2020, Klemm *et al.* 2021). Wing measurements were performed by removing wings, mounting in Permount solution (Fisher Scientific) and imaged using a Zeiss Discovery.V8 microscope. Wing area was measured using the Fiji software. Male and female adults were measured separately to account for sex differences in wing size

using a reproducible measuring protocol that excludes the variable hinge region of the wing (details of measuring protocol available on request). Statistics were performed using GraphPad Prism 10.0.

Immunohistochemistry

Larvae were dissected in 1 x PBS followed by a 20 min fix in 4 % paraformaldehyde in PBS (PFA). After 3 washes in 0.1 % PBST (1 x PBS + 0.1 % Triton-X), larvae were washed in 0.3% PBST and then blocked in 0.1 % PBST with 5 % normal goat serum (NGS) for 30 min. Primary staining was done overnight at 4°C, and secondary staining was done for 4 hr at room temperature. The following primary antibodies were obtained from the Developmental Studies Hybridoma Bank: mouse anti-Nubbin (1:25), mouse anti-Wg (1:100), mouse anti-Mmp1 C-terminus (1:100), mouse anti-Mmp1 catalytic domain (1:100), mouse anti-LacZ (1:100), mouse anti-discs large (1:50), mouse anti-yH2Av (1:100), and rat anti-DE-cadherin (1:100). Rabbit anti-Dcp-1 (1:1000), mouse anti-PH3 (1:500), and rabbit anti-HA (1:1000) were obtained from Cell Signaling Technologies. Rat anti-Zfh-2 was generously gifted by Chris Doe. Anti-rabbit 647, anti-rat 647, anti-mouse 555, and anti-mouse 488 secondary antibodies were obtained from Invitrogen and used at a 1:500 dilution. DAPI (1:1000) was used as a counterstain. Images were obtained on a Zeiss AxioImager.M2 with ApoTome and a Leica TCS SP8 LCSM (NIH SIG award 1 S10 OD023691-01) housed in the Regenerative Medicine Imaging Facility at Arizona State University. For each experiment at least 15 discs were analyzed prior to choosing a representative image. Images were processed using Affinity Photo.

EdU staining, TUNEL assay, and DHE staining

EdU. The Click-It EdU Alexa Fluor 555 Imaging Kit (Invitrogen C10338) was used to assay cell proliferation. Briefly, imaginal discs were dissected and labeled with 1 µl EdU in 1 ml PBS for 20 min, fixed in 4 % PFA for 20 min and immunolabeled (as necessary), followed by a 30 min Click-It reaction that was performed as directed in the EdU manual.

TUNEL. The TUNEL assay was performed with the ApopTag Red In Situ Apoptosis Detection Kit (Millipore S7165). Dissected larvae were fixed in 4 % paraformaldehyde, followed by a 10 min wash in 75 ml equilibration buffer. Discs were then submerged in 55 ml working strength TdT enzyme for 3 hr at 37°C. The reaction was stopped by adding 1ml stop/wash buffer and incubating for 10min at room temperature, followed by three washes in PBS. Immunolabeling was performed by incubating the tissue preps with 65 ml of anti-digoxigenin rhodamine overnight at room temperature.

Dihydroethidium (DHE). DHE labeling was performed by incubating freshly dissected wing imaginal discs in Schneider's Media with 1 µl of 10 mM DHE reconstituted in 1 ml DMSO (for a working concentration of 10 µm DHE) for 10 min, followed by three 5 min washes in PBS and immediately mounting and imaging.

Quantification and Statistical Analysis

Adult wings, mean fluorescence intensity, and cell counts were measured using Fiji. GraphPad Prism 10.0 was used for statistical analysis and graphical representation. Graphs depict the mean of each treatment, while error bars represent the standard deviation. The mean fluorescence intensity of EdU labeling was quantified in Fiji by normalizing the wing pouch to the entire disc. The sample size and P values for all statistical analyses are indicated in the figure legends. Statistical significance was evaluated in Prism 10.0 using a Student's T-test or a one-way ANOVA with a multiple comparisons test.

Data and reagent availability

Stocks are available upon request and details of stocks and reagents used in this study are available in the materials and methods. The authors affirm that all data necessary for confirming the conclusions of the article are present within the article, figures, and tables.

Acknowledgements

The authors would like to thank Dr. Tin Tin Su of UC Boulder, Dr. Chris Doe of the University of Oregon, and Dr. Tian Xie of the Stowers Institute for their generous gift of stocks and reagents. We thank the current members of the Harris lab for useful input and feedback. We thank the Bloomington Drosophila Stock Center and Developmental Studies Hybridoma Bank for stocks and reagents.

Funding

This work was supported by a grant from the Eunice Kennedy Shriver National Institute of Child Health and Human Development (NICHD) R21HD102765-01 and the National Institute of General Medical Sciences (NIGMS) R01GM147615 to Robin Harris.

Author contributions

Jacob Klemm, Conceptualization, Investigation, Data curation, Formal analysis, Validation, Writing – original draft, Writing – review and editing; Chloe Van Hazel, Resources; Robin Harris, Supervision, Conceptualization, Funding acquisition, Investigation, Resources, Writing – review and editing.

Conflicts of interest

The authors declare that there is no conflict of interest.

References

1. Amcheslavsky, A., et al. (2018). "Plasma Membrane Localization of Apoptotic Caspases for Non-apoptotic Functions." *Dev Cell* **45**(4): 450-464 e453.

2. Anthoney, N., et al. (2018). "Toll and Toll-like receptor signalling in development." *Development* **145**(9).

3. Ashkenazi, A. and G. Salvesen (2014). "Regulated cell death: signaling and mechanisms." *Annu Rev Cell Dev Biol* **30**: 337-356.

4. Bach, E. A., et al. (2007). "GFP reporters detect the activation of the Drosophila JAK/STAT pathway in vivo." *Gene Expr Patterns* **7**(3): 323-331.

5. Baena-Lopez, L. A., et al. (2018). "Novel initiator caspase reporters uncover previously unknown features of caspase-activating cells." *Development* **145**(23).

6. Bardet, P. L., et al. (2008). "A fluorescent reporter of caspase activity for live imaging." *Proc Natl Acad Sci U S A* **105**(37): 13901-13905.

7. Beira, J. V. and R. Paro (2016). "The legacy of Drosophila imaginal discs." *Chromosoma* **125**(4): 573-592.

8. Bergmann, A. and H. Steller (2010). "Apoptosis, stem cells, and tissue regeneration." *Sci Signal* **3**(145): re8.

9. Bonne, S. L. and S. S. Kadri (2017). "Evaluation and Management of Necrotizing Soft Tissue Infections." *Infect Dis Clin North Am* **31**(3): 497-511.

10. Brown-Suedel, A. N. and L. Bouchier-Hayes (2020). "Caspase-2 Substrates: To Apoptosis, Cell Cycle Control, and Beyond." *Front Cell Dev Biol* **8**: 610022.

11. Cao, X. (2016). "Self-regulation and cross-regulation of pattern-recognition receptor signalling in health and disease." *Nat Rev Immunol* **16**(1): 35-50.

12. Chatterjee, N. and D. Bohmann (2012). "A versatile PhiC31 based reporter system for measuring AP-1 and Nrf2 signaling in Drosophila and in tissue culture." *PLoS One* **7**(4): e34063.

13. Chera, S., et al. (2009). "Apoptotic cells provide an unexpected source of Wnt3 signaling to drive hydra head regeneration." *Dev Cell* **17**(2): 279-289.

14. Colon Plaza, S. and T. T. Su (2024). "Ionizing radiation induces cells with past caspase activity that contribute to the adult organ in Drosophila and show reduced Loss of Heterozygosity." *Cell Death Discov* **10**(1): 6.

15. D'Arcy, M. S. (2019). "Cell death: a review of the major forms of apoptosis, necrosis and autophagy." *Cell Biol Int* **43**(6): 582-592.

16. Ding, A. X., et al. (2016). "CasExpress reveals widespread and diverse patterns of cell survival of caspase-3 activation during development in vivo." *Elife* **5**.

17. Diwanji, N. and A. Bergmann (2018). "An unexpected friend - ROS in apoptosis-induced compensatory proliferation: Implications for regeneration and cancer." *Semin Cell Dev Biol* **80**: 74-82.

18. Evans, C. J., et al. (2009). "G-TRACE: rapid Gal4-based cell lineage analysis in Drosophila." *Nat Methods* **6**(8): 603-605.

19. Fan, Y. and A. Bergmann (2008). "Apoptosis-induced compensatory proliferation. The Cell is dead. Long live the Cell!" *Trends Cell Biol* **18**(10): 467-473.

20. Fan, Y. and A. Bergmann (2008). "Distinct mechanisms of apoptosis-induced compensatory proliferation in proliferating and differentiating tissues in the Drosophila eye." *Dev Cell* **14**(3): 399-410.

21. Fan, Y., et al. (2014). "Genetic models of apoptosis-induced proliferation decipher activation of JNK and identify a requirement of EGFR signaling for tissue regenerative responses in Drosophila." *PLoS Genet* **10**(1): e1004131.

22. Festjens, N., et al. (2006). "Necrosis, a well-orchestrated form of cell demise: signalling cascades, important mediators and concomitant immune response." *Biochim Biophys Acta* **1757**(9-10): 1371-1387.

23. Florentin, A. and E. Arama (2012). "Caspase levels and execution efficiencies determine the apoptotic potential of the cell." *J Cell Biol* **196**(4): 513-527.

24. Fogarty, C. E. and A. Bergmann (2017). "Killers creating new life: caspases drive apoptosis-induced proliferation in tissue repair and disease." *Cell Death Differ* **24**(8): 1390-1400.

25. Fogarty, C. E., et al. (2016). "Extracellular Reactive Oxygen Species Drive Apoptosis-Induced Proliferation via Drosophila Macrophages." *Curr Biol* **26**(5): 575-584.

26. Fox, D. T., et al. (2020). "Model systems for regeneration: Drosophila." *Development* **147**(7).

27. Fuchs, Y. and H. Steller (2015). "Live to die another way: modes of programmed cell death and the signals emanating from dying cells." *Nat Rev Mol Cell Biol* **16**(6): 329-344.

28. Gong, T., et al. (2020). "DAMP-sensing receptors in sterile inflammation and inflammatory diseases." *Nat Rev Immunol* **20**(2): 95-112.

29. Gordon, O., et al. (2018). "alpha-actinin accounts for the bioactivity of actin preparations in inducing STAT target genes in Drosophila melanogaster." *Elife* **7**.

30. Grasl-Kraupp, B., et al. (1995). "In situ detection of fragmented DNA (TUNEL assay) fails to discriminate among apoptosis, necrosis, and autolytic cell death: a cautionary note." *Hepatology* **21**(5): 1465-1468.

31. Hajibabaie, F., et al. (2023). "Types of Cell Death from a Molecular Perspective." *Biology (Basel)* **12**(11).

32. Hakkarainen, T. W., et al. (2014). "Necrotizing soft tissue infections: review and current concepts in treatment, systems of care, and outcomes." *Curr Probl Surg* **51**(8): 344-362.

33. Hariharan, I. K. and F. Serras (2017). "Imaginal disc regeneration takes flight." *Curr Opin Cell Biol* **48**: 10-16.

34. Harris, R. E. (2023). "Investigating Tissue Regeneration Using the DUAL Control Genetic Ablation System." *Methods Mol Biol* **2599**: 255-270.

35. Harris, R. E., et al. (2020). "Damage-responsive, maturity-silenced enhancers regulate multiple genes that direct regeneration in Drosophila." *Elife* **9**.

36. Hay, B. A., et al. (1994). "Expression of baculovirus P35 prevents cell death in Drosophila." *Development* **120**(8): 2121-2129.

37. Herrera, S. C. and E. A. Bach (2019). "JAK/STAT signaling in stem cells and regeneration: from Drosophila to vertebrates." *Development* **146**(2).

38. Huh, J. R., et al. (2004). "Compensatory proliferation induced by cell death in the Drosophila wing disc requires activity of the apical cell death caspase Dronc in a nonapoptotic role." *Curr Biol* **14**(14): 1262-1266.

39. Jaiswal, J., et al. (2023). "Mutual repression between JNK/AP-1 and JAK/STAT stratifies senescent and proliferative cell behaviors during tissue regeneration." *PLoS Biol* **21**(5): e3001665.
40. Jung, Y., et al. (2010). "Signals from dying hepatocytes trigger growth of liver progenitors." *Gut* **59**(5): 655-665.
41. Kamber Kaya, H. E., et al. (2017). "An inhibitory mono-ubiquitylation of the Drosophila initiator caspase Dronc functions in both apoptotic and non-apoptotic pathways." *PLoS Genet* **13**(2): e1006438.
42. Karsch-Bluman, A., et al. (2019). "Tissue necrosis and its role in cancer progression." *Oncogene* **38**(11): 1920-1935.
43. Katsuyama, T., et al. (2015). "During Drosophila disc regeneration, JAK/STAT coordinates cell proliferation with Dilp8-mediated developmental delay." *Proc Natl Acad Sci U S A* **112**(18): E2327-2336.
44. Khan, S. J., et al. (2017). "The Drosophila Duox maturation factor is a key component of a positive feedback loop that sustains regeneration signaling." *PLoS Genet* **13**(7): e1006937.
45. Kim, J., et al. (1996). "Integration of positional signals and regulation of wing formation and identity by Drosophila vestigial gene." *Nature* **382**(6587): 133-138.
46. Klemm, J., et al. (2021). "Necrosis-induced apoptosis promotes regeneration in Drosophila wing imaginal discs." *Genetics* **219**(3).
47. Konstantinidis, K., et al. (2012). "Mechanisms of cell death in heart disease." *Arterioscler Thromb Vasc Biol* **32**(7): 1552-1562.
48. La Fortezza, M., et al. (2016). "JAK/STAT signalling mediates cell survival in response to tissue stress." *Development* **143**(16): 2907-2919.
49. La Marca, J. E. and H. E. Richardson (2020). "Two-Faced: Roles of JNK Signalling During Tumourigenesis in the Drosophila Model." *Front Cell Dev Biol* **8**: 42.
50. Ledru, M., et al. (2022). "Differential gene expression analysis identified determinants of cell fate plasticity during radiation-induced regeneration in Drosophila." *PLoS Genet* **18**(1): e1009989.
51. Li, F., et al. (2010). "Apoptotic cells activate the "phoenix rising" pathway to promote wound healing and tissue regeneration." *Sci Signal* **3**(110): ra13.
52. Li, M., et al. (2019). "Characterization of TNF-induced cell death in Drosophila reveals caspase- and JNK-dependent necrosis and its role in tumor suppression." *Cell Death Dis* **10**(8): 613.
53. Li, Z., et al. (2023). "Advances in experimental models of osteonecrosis of the femoral head." *J Orthop Translat* **39**: 88-99.
54. Liu, K., et al. (2013). "Modeling calcium-overload mediated necrosis in Drosophila." *Methods Mol Biol* **1004**: 203-213.
55. Madigan, J. P., et al. (2002). "DNA double-strand break-induced phosphorylation of Drosophila histone variant H2Av helps prevent radiation-induced apoptosis." *Nucleic Acids Res* **30**(17): 3698-3705.
56. Martin, R., et al. (2017). "Distinct regenerative potential of trunk and appendages of Drosophila mediated by JNK signalling." *Development* **144**(21): 3946-3956.
57. Masi, L., et al. (2007). "Osteonecrosis in genetic disorders." *Clin Cases Miner Bone Metab* **4**(1): 27-29.

58. Meier, P., et al. (2000). "The Drosophila caspase DRONC is regulated by DIAP1." *EMBO J* **19**(4): 598-611.
59. Ming, M., et al. (2014). "Persephone/Spatzle pathogen sensors mediate the activation of Toll receptor signaling in response to endogenous danger signals in apoptosis-deficient Drosophila." *J Biol Chem* **289**(11): 7558-7568.
60. Morata, G., et al. (2011). "Mitogenic signaling from apoptotic cells in Drosophila." *Dev Growth Differ* **53**(2): 168-176.
61. Mulay, S. R., et al. (2016). "Necroinflammation in Kidney Disease." *J Am Soc Nephrol* **27**(1): 27-39.
62. Nakada, H., et al. (2019). "Fat necrosis after breast-conserving oncoplastic surgery." *Breast Cancer* **26**(1): 125-130.
63. Nano, M. and D. J. Montell (2024). "Apoptotic signaling: Beyond cell death." *Semin Cell Dev Biol* **156**: 22-34.
64. Nishida, H., et al. (2024). "Necrosensor: a genetically encoded fluorescent sensor for visualizing necrosis in Drosophila." *Biol Open* **13**(1).
65. Pellettieri, J., et al. (2010). "Cell death and tissue remodeling in planarian regeneration." *Dev Biol* **338**(1): 76-85.
66. Perez-Garijo, A. (2018). "When dying is not the end: Apoptotic caspases as drivers of proliferation." *Semin Cell Dev Biol* **82**: 86-95.
67. Perez-Garijo, A., et al. (2004). "Caspase inhibition during apoptosis causes abnormal signalling and developmental aberrations in Drosophila." *Development* **131**(22): 5591-5598.
68. Perez-Garijo, A., et al. (2005). "Dpp signaling and the induction of neoplastic tumors by caspase-inhibited apoptotic cells in Drosophila." *Proc Natl Acad Sci U S A* **102**(49): 17664-17669.
69. Perez-Garijo, A., et al. (2009). "The role of Dpp and Wg in compensatory proliferation and in the formation of hyperplastic overgrowths caused by apoptotic cells in the Drosophila wing disc." *Development* **136**(7): 1169-1177.
70. Perez-Garijo, A. and H. Steller (2015). "Spreading the word: non-autonomous effects of apoptosis during development, regeneration and disease." *Development* **142**(19): 3253-3262.
71. Pinal, N., et al. (2019). "Pro-apoptotic and pro-proliferation functions of the JNK pathway of Drosophila: roles in cell competition, tumorigenesis and regeneration." *Open Biol* **9**(3): 180256.
72. Pinal, N., et al. (2018). "Short-term activation of the Jun N-terminal kinase pathway in apoptosis-deficient cells of Drosophila induces tumorigenesis." *Nature Communications* **9**(1).
73. Robertson, S. A., et al. (2017). "Mastectomy skin flap necrosis: challenges and solutions." *Breast Cancer (Dove Med Press)* **9**: 141-152.
74. Roh, J. S. and D. H. Sohn (2018). "Damage-Associated Molecular Patterns in Inflammatory Diseases." *Immune Netw* **18**(4): e27.
75. Ryoo, H. D. and A. Bergmann (2012). "The role of apoptosis-induced proliferation for regeneration and cancer." *Cold Spring Harb Perspect Biol* **4**(8): a008797.
76. Ryoo, H. D., et al. (2004). "Apoptotic cells can induce compensatory cell proliferation through the JNK and the Wingless signaling pathways." *Dev Cell* **7**(4): 491-501.

77. Schott, S., et al. (2017). "A fluorescent toolkit for spatiotemporal tracking of apoptotic cells in living Drosophila tissues." *Development* **144**(20): 3840-3846.

78. Shapiro, P. J., et al. (2008). "Regulation of the Drosophila apoptosome through feedback inhibition." *Nat Cell Biol* **10**(12): 1440-1446.

79. Shinoda, N., et al. (2019). "Dronc-independent basal executioner caspase activity sustains Drosophila imaginal tissue growth." *Proc Natl Acad Sci U S A* **116**(41): 20539-20544.

80. Siegrist, S. E., et al. (2010). "Inactivation of both Foxo and reaper promotes long-term adult neurogenesis in Drosophila." *Curr Biol* **20**(7): 643-648.

81. Su, T. T. (2020). "Non-apoptotic roles of apoptotic proteases: new tricks for an old dog." *Open Biol* **10**(8): 200130.

82. Tonnus, W., et al. (2021). "The role of regulated necrosis in endocrine diseases." *Nat Rev Endocrinol* **17**(8): 497-510.

83. Tseng, A. S., et al. (2007). "Apoptosis is required during early stages of tail regeneration in Xenopus laevis." *Dev Biol* **301**(1): 62-69.

84. Venereau, E., et al. (2015). "DAMPs from Cell Death to New Life." *Front Immunol* **6**: 422.

85. Verghese, S. and T. T. Su (2016). "Drosophila Wnt and STAT Define Apoptosis-Resistant Epithelial Cells for Tissue Regeneration after Irradiation." *PLoS Biol* **14**(9): e1002536.

86. Verghese, S. and T. T. Su (2018). "Ionizing radiation induces stem cell-like properties in a caspase-dependent manner in Drosophila." *PLoS Genet* **14**(11): e1007659.

87. Vriz, S., et al. (2014). "Cell death: a program to regenerate." *Curr Top Dev Biol* **108**: 121-151.

88. Wang, L. H. and N. E. Baker (2019). "Salvador-Warts-Hippo pathway regulates sensory organ development via caspase-dependent nonapoptotic signaling." *Cell Death Dis* **10**(9): 669.

89. Worley, M. I. and I. K. Hariharan (2022). "Imaginal Disc Regeneration: Something Old, Something New." *Cold Spring Harb Perspect Biol* **14**(11).

90. Worley, M. I., et al. (2012). "Regeneration and transdetermination in Drosophila imaginal discs." *Annu Rev Genet* **46**: 289-310.

91. Wu, M. Y., et al. (2018). "Current Mechanistic Concepts in Ischemia and Reperfusion Injury." *Cell Physiol Biochem* **46**(4): 1650-1667.

92. Xu, D., et al. (2005). "The CARD-carrying caspase Dronc is essential for most, but not all,developmental cell death inDrosophila." *Development* **132**(9): 2125-2134.

93. Yang, X., et al. (2021). "Treatment of Radiation-Induced Brain Necrosis." *Oxid Med Cell Longev* **2021**: 4793517.

94. Yang, Y., et al. (2013). "Neuronal necrosis and spreading death in a Drosophila genetic model." *Cell Death Dis* **4**: e723.

Article and author information

Jacob Klemm

School of Life Sciences, Arizona State University, Life Sciences E (LSE) 354, 427 Tyler Mall, Tempe, Arizona, 85287-4501

jwklemm@asu.edu

ORCID iD: 0000-0002-1414-5089

Chloe Van Hazel

School of Life Sciences, Arizona State University, Life Sciences E (LSE) 354, 427 Tyler Mall, Tempe, Arizona, 85287-4501

Robin Harris

School of Life Sciences, Arizona State University, Life Sciences E (LSE) 354, 427 Tyler Mall, Tempe, Arizona, 85287-4501

For correspondence: reharri4@asu.edu

ORCID iD: 0000-0001-6945-6741

Figure Legends

Figure 1. The NiA response is restricted to pouch cells following ablation. (**A**) A schematic of the *DC*^{GluR1} ablation scheme. This system utilizes a split LexA transcriptional activator that promotes the expression of *lexAop-GluR1* following a short heat shock (45 min at 37°C). (**B**) A schematic of the different tissue domains and compartments targeted for *GAL4/UAS/GAL80*^{ts} (*GAL4*^{ts}) ablation. (**C**) A schematic of the temperature scheme used to induce necrosis with *GAL4*^{ts}*>GluR1* following the heat shift (20 hr at 30°C) induced inactivation of *GAL80*^{ts}. (**D**) A control disc for DUAL Control (*DC*^{NA}) experiments bearing *lexAop-GFP*, which labels the domain targeted for ablation with *DC*^{GluR1}. (**E**) A *DC*^{GluR1} ablated disc at 18 hr of regeneration bearing *lexAop-GFP*, yellow arrowheads indicate pouch NiA, red arrowhead indicates a cluster of Dcp-1-positive cells in the posterior pleura. (**F**) A control disc for *R85E08-GAL4*^{ts} (*R85*^{ts}*>GFP*) ablation. (**G**) An *R85E08*^{ts}*>GluR1,GFP* ablated disc, arrowheads indicate the presence of NiA cells following ablation. (**H**) A control disc for whole pouch (*rn*^{ts}*>GFP*) ablation. (**I-J**) A *rn*^{ts}*>GluR1,GFP* ablated disc dissected immediately following the downshift (0 hr, **I**) and after 24 hr of regeneration (R24, **J**). (**K**) A control disc for notum ablation (*pnr*^{ts}*>GFP*). (**L-M**) *pnr*^{ts}*>GluR1,GFP* ablated discs at 0 hr (**L**) and 24 hr (**M**), open arrowheads highlight the absence of the Wg notum stripe following ablation. (**N**) A control disc for hinge ablation (*R73G07ts>GFP*). (**O-P**) *R73G08*^{ts}*>GluR1,GFP* ablated discs at 0 hr (**O**) and 24 hr (**P**). Open arrowhead in (**O**) indicates the absence of NiA in the adjacent wing pouch. (**Q**) A control disc for posterior compartment ablation (*hh*^{ts}*>GFP*). (**R-S'**) *hh*^{ts}*>GluR1,GFP* ablated discs at 0 hr (**R-R'**) and 24 hr (**S-S'**). Dotted lines in (**R'**) and (**S'**) show an absence of NiA in the anterior hinge. (**T**) A quantification of the NiA response in the anterior pouch, hinge, and notum in control (n= 13), 0 hr (n= 14), and 24 hr (n= 12) discs in response to *hh* ablation. NiA are defined as Dcp-1-positive (Dcp-1+ve), GFP-negative (GFP-ve) cells. See Supplementary Genotypes file for exact genotypes.

Figure 1 – figure supplement 1. (**A**) A *nub*^{ts}*>GluR1,GFP* ablated disc at 0 hr. (**B**) A *DC*^{GluR1} ablated disc highlighting the overlap between wound edge apoptosis and the JNK target Mmp1 (arrowhead). (**C**) A control disc for anterior compartment ablation (*ptc*^{ts}*>RFP*). (**D-E'**) *ptc*^{ts}*>GluR1,RFP* ablated discs at 0 hr (**D-D'**) and 24 hr (**E-E'**). Dotted lines in (**D'**) and (**E'**) highlight the lack of NiA cells in the hinge. (**F**) A quantification of the NiA response to *ptc* ablation in the pouch, hinge, and notum of control (n= 14), 0 hr (n= 15), and 24 hr (n= 14) discs, with NiA being defined as Dcp-1-positive (+ve), RFP-negative (-ve) cells. (**G**) A control disc for *FLP/FRT* clonal ablation, where actin-FRT>stop>FRT-GAL-4 (*act*^{ts}*>>RFP*) drives the expression of *UAS-RFP* in clonal patches of cells after a short heat shock (see materials and methods for details). (**H-H''**) A wing disc with clonal patches of *UAS-RFP*, *UAS-GluR1* expressing cells. (**H'**) is a zoom-in of pouch and hinge clones with arrowheads pointing to NiA cells, while (**H''**) is a zoom-in of notum clones. (**I**) A quantification of the number of NiA cells induced following ablation with *act*^{ts}*>>GluR1* (n= 11), *R85E08*^{ts}*>GluR1* (n= 10), *ptc*^{ts}*>GluR1* (n= 15), and *hh*^{ts}*>GluR1* (n= 14), highlighting that NiA number increases with increasing area of ablation. See Supplementary Genotypes file for exact genotypes.

Figure 2. NiA formation in pouch cells is regulated by the Wg and JAK/STAT pathways. (**A**). A control disc (DC^{NA}) bearing the *10xSTAT-GFP* reporter, showing the hinge-specific Stat92E activity that is normally absent from the wing pouch. (**B**) A DC^{GluR1} ablated disc bearing *10xSTAT-GFP*. Following damage, pouch-specific reporter expression is observed at high levels at the wound edge (arrowhead) and low levels at the NiA area of the pouch (open arrowhead). (**C-E**) DC^{GluR1}>>y^{RNAi} (**C**, n=14) versus DC^{GluR1}>>$dome^{RNAi}$ (**D**, n=14) ablated discs, with the number of Dcp-1+ve cells in the WE vs LP quantified in (**E**), P**** <0.0001. Data were analyzed with a one-way ANOVA followed by a multiple comparisons test. (**F**) A DC^{GluR1}*hh-GAL4* ablation schematic ($DC^{GluR1}hh^{ts}$). A short heat shock (45 min at 37°C) induces split *LexA/lexAop-GluR1* ablation, while a heat shift (18 hr at 30°C) following the heat shock will inactivate $GAL80^{ts}$ and permit *UAS-X* expression. (**G**) A $DC^{GluR1}hh^{ts}$>*GFP* ablated disc, where GFP highlights the area of the disc being targeted for JAK/STAT and Wg knockdown in the following experiments. The posterior NiA will be assayed in response to knockdown while anterior NiA serve as an internal control. (**H**) A control hh^{ts}>*GFP,*$Stat92E^{RNAi}$ disc showing no changes in cell death. (**I**) A $DC^{GluR1}hh^{ts}$>$Stat92E^{RNAi}$ ablated disc, arrowhead highlights an increase in pouch NiA. (**J**) A control DC^{NA} disc showing developmental Wg expression. (**K**) A DC^{GluR1}>>y^{RNAi} ablated disc showing that NiA cells avoid the areas of the pouch with high Wg expression, while wound edge apoptotic cells overlap the developmental and damage-specific Wg-expressing cells (arrowhead). (**L**) A control hh^{ts}>*GFP,*wg^{RNAi} disc showing the absence of Wg in the posterior pouch and no change in posterior cell death. (**M**) A $DC^{GluR1}hh^{ts}$>wg^{RNAi} ablated disc with NiA cells observed at the posterior margin (arrowhead) while anterior NiA avoid the Wg margin stripe (open arrowhead). See Supplementary Genotypes file for exact genotypes.

Figure 2 – figure supplement 1. (**A**) A *DC*^{NA}*>>hop48A* control disc with high levels of Dcp-1 observed throughout the pouch. (**B**) A *DC*^{GluR1}*>>hop48A* ablated disc with high levels of apoptosis throughout the pouch, likely due to *UAS-hop48A* expression (**A**). (**C**) A *DC*^{GluR1}*hh*^{ts}*>GFP* ablated disc with nubbin and DCAD highlighting the ablated *salm* domain and GFP labeling the area of *UAS-X* expression. (**D**) A control *hh*^{ts}*>GFP,Zfh2*^{RNAi} disc showing no changes in cell death. (**E**) A *DC*^{GluR1}*hh*^{ts}*>Zfh2*^{RNAi} ablated disc showing a slight increase in pouch NiA. (**F**) A control disc bearing the *vgQE-lacZ* reporter showing the area of the pouch with vestigial quadrant enhancer expression. (**G**) A *DC*^{GluR1} ablated disc bearing *vgQE-lacZ*, showing the high degree of overlap between NiA cells and lacZ-expressing cells. (**H**) A control *hh*^{ts}*>Wg* disc with no strong changes in cell death observed. (**I**) A *DC*^{GluR1}*hh*^{ts}*>Wg* ablated disc showing an increase in apoptosis across the wing pouch and in the posterior pleura. See Supplementary Genotypes file for exact genotypes.

Figure 3. NiA promotes proliferation late in regeneration. (**A-A'''**) A time course of *DC*^{GluR1} ablated discs bearing the *PCNA-GFP* reporter at 18 hr (**A**), 24 hr (**A'**), 36 hr (**A''**), and 48 hr (**A'''**). (**B-B'''**) A time course of *DC*^{GluR1}*>>y*^{RNAi} ablated discs at 18 hr (**B**), 24 hr (**B'**), 36 hr (**B''**), and 48 hr (**B'''**). High levels of EdU are observed by 36 hr that remain elevated at 48 hr. (**C-C'''**) A time course of *DC*^{hepCA}*>>y*^{RNAi} ablated discs at 18 hr (**C**), 24 hr (**C'**), 36 hr (**C''**), and 48 hr (**C'''**). (**D-D'''**) A time course of *DC*^{GluR1}*>>mir(RHG)* ablated discs at 18 hr (**D**), 24 hr (**D'**), 36 hr (**D''**), and 48 hr (**D'''**). (**E**) A graph of the *DC*^{GluR1}, *DC*^{hepCA}, and *DC*^{NA} EdU time courses highlight the pattern of EdU labeling in the wing pouch between each system. (**F**) A quantification of EdU signal intensity between *DC*^{GluR1}*>>y*^{RNAi} at 18 hr (n= 10), 24 hr (n= 10), 36 hr (n= 10), 48 hr (n= 10), and *DC*^{GluR1}*>>mir(RHG)* at 18 hr (n= 10), 24 hr (n= 8), 36 hr (n= 11), and 48 hr (n= 10) time courses, ns, not significant; ***P = 0.0002; ****P <0.0001; data were analyzed with a one-way ANOVA and multiple comparisons test. (**G-J**) *DC*^{GluR1} ablated discs with different populations of apoptotic cells suppressed by *mir(RHG)*. (**G**) A control *DC*^{GluR1}*>>y*^{RNAi} ablated disc showing the typical pattern of NiA formation. (**H**) A *DC*^{GluR1}*>>mir(RHG)* ablated disc suppressing both wound edge apoptosis and NiA cells. (**I**) A *DC*^{GluR1}*>>miRHG;DR*^{WNT}*-GAL80* ablated disc, which targets the LP for *UAS-mir(RHG)* expression (*LP>mir(RHG)*). (**J**) A *DC*^{GluR1} *x R85E08>mir(RHG)* ablated disc, which targets the WE for suppression (*WE>mir(RHG)*). The dotted lines each panel highlight the area of *UAS-mir(RHG)* expression. (**K-N**) *DC*^{GluR1} ablated discs with representative EdU labels at R36 in response to *y*^{RNAi} (**K**), whole-pouch *mir(RHG)* (**L**), *LP>mir(RHG)* (**M**), and *WE>mir(RHG)* (**N**). (**O**) A quantification of the normalized EdU fluorescent intensity of *DC*^{GluR1}*>>y*^{RNAi} 18 hr (n= 10), *DC*^{GluR1}*>>y*^{RNAi} 36 hr (n= 10), *DC*^{GluR1}*>>mir(RHG*) 36 hr (n= 11), *LP>mir(RHG)* 36 hr (n= 10), and *WE>mir(RHG)* 36 hr (n= 9) ablated discs; *P = 0.0189, **P = 0.0044, ***P = 0.0008, ****P < 0.0001; data were analyzed with a one-way ANOVA and multiple comparisons tests. LP = lateral pouch, WE = wound edge. See Supplementary Genotypes file for exact genotypes.

Figure 3 – figure supplement 1. (**A-A'''**) A *DC*^{NA}*>>y*^{RNAi} control time course at 18 hr (**A**), 24 hr (**A'**), 36 hr (**A''**), and 48 hr (**A'''**). The folds of the wing pouch were used to outline the EdU signal for quantification in all experiments, as visualized by DAPI. (**B-C**) A *DC*^{NA}*>>y*^{RNAi} control disc (**B**) with EdU labeling relative to a *DC*^{NA}*>>mir(RHG)* control disc (**C**). (**D**) A quantification of discs in (**B**, n=10) and (**C**, n=10) demonstrating that miRHG expression does not alter EdU levels, ns, not significant. Data were analyzed with a Student's T-test. See Supplementary Genotypes file for exact genotypes.

Figure 4 NiA promote proliferation independent of Apoptosis-induced Proliferation (AiP). (**A-A'**) A *DC*^{NA} control disc bearing the *wg-lacZ* reporter. (**B-B'**) A *DC*^{GluR1} ablated disc with *wg-lacZ* showing the expression of the reporter during regeneration, with lacZ-expressing cells at the wound edge. The 24 hr time point was chosen as an intermediate between NiA formation (18 hr) and blastema formation (36 hr), when secreted factors are likely to be detected. (**C-C'**) A *DC*^{GluR1}*>>P35* ablated disc bearing *wg-lacZ* with lac-Z expressing cells observed at the WE (arrowhead) but not in the LP (open arrowhead). (**D-D'**) A *DC*^{NA} control disc bearing the *dpp-lacZ* reporter. (**E-E'**) A *DC*^{GluR1} ablated disc with *dpp-lacZ*, with lac-Z expressing cells observed at the WE. (**F-F'**) A *DC*^{GluR1}*>>P35* ablated disc bearing *dpp-lacZ*, with lacZ expressing cells at the WE (arrowhead) but not the LP (open arrowhead). (**G**) A *DC*^{GluR1} ablated disc bearing the transcriptional *AP-1-GFP* reporter and labeled with dihydroethidium (DHE). Low levels of DHE labeling are observed at the WE, where AP-1-GFP expression occurs (arrowhead), while no DHE labeling is observed in the LP. (**H**) A *DC*^{GluR1}*>>Cat,Sod1* ablated disc showing reduced WE apoptosis (open arrowhead) but no change in NiA formation. (**I**) A *DC*^{GluR1}*>>Duox*^{RNAi} ablated disc showing a similar pattern to (**H**) with an observed loss of WE apoptosis (open arrowhead) but no change in NiA formation. (**J-L**) *DC*^{GluR1} ablated discs bearing *yRNAi* (**J**), *P35* (**K**), and *LP>P35* (**L**) at 36 hr and labeled with EdU. (**M**) A quantification of discs in (**J-L**) demonstrate no change in EdU labeling upon the expression of P35 in the LP (*LP>P35*, **L**), confirming that NiA promote proliferation independent of AiP, ns, not significant. Data were analyzed with a one-way ANOVA followed by a multiple comparisons test. LP = lateral pouch, AiP = apoptosis-induced proliferation. See Supplementary Genotypes file for exact genotypes.

Figure 4 – figure supplement 1. (**A**) A *DC*^{NA} control disc bearing the *spi-lacZ* reporter, showing no lacZ expression in the wing disc. (**B**) A *DC*^{GluR1}*>>P35* ablated disc bearing *spi-lacZ* showing a few lac-Z-expressing cells at the WE. (**C**) A *DC*^{NA} control disc bearing *mol-lacZ* highlighting the developmental expression pattern of *mol* in the wing disc. (**D**) A *DC*^{GluR1} ablated disc bearing *mol-lacZ*, with a slight increase in lacZ expression observed at the WE (arrowhead). See Supplementary Genotypes file for exact genotypes.

Figure 5. NiCP cells persist in the disc proper throughout regeneration. (**A-D**) A time course of *DC*^{GluR1} ablated discs bearing the fluorescent caspase reporter *UAS-GC3Ai* at 18 hr (**A**), 24 hr (**B**), 36 hr (**C**), and 48 hr (**D**). (**E**) A *DC*^{GluR1}*>>GC3Ai* ablated disc at 64 hr, with GC3Ai-positive cells present at the WE after the nubbin marker is reestablished (arrowhead). (**F-F'**) A *DC*^{GluR1}*>>GC3Ai* ablated disc at 36 hr with GC3Ai-positive cells associated with the mitotic PH3 marker. Yellow arrowhead in (**F'**) points to cytoplasmic, undisturbed cells, while the red arrowhead points to cells with a pyknotic morphology. (**G-H**) A *DC*^{GluR1} *LP>GC3Ai* ablated disc at 18 hr (**G**) and 36 hr (**H**). The arrowhead in (**H**) highlights the presence of GC3Ai-labeled NiA cells at the WE. (**I-I'**) A *DC*^{hepCA}*>>GC3Ai* ablated disc at 18 hr with apoptotic cells present throughout the disc proper. (**J-J'**) A *DC*^{hepCA}*>>GC3Ai* ablated disc at 36 hr (**J**) and 64 hr (**J'**); all apoptotic cells appear to be pushed out towards the basal surface of the disc proper. (**K-K'**) A *DC*^{GluR1}*>>GC3Ai* ablated discs at 18 hr with NiA cells present in the disc proper. (**L-L'**) A *DC*^{GluR1} *LP>GC3Ai* ablated disc at 36 hr, with columnar-shaped GC3Ai-positive cells in the disc proper (yellow arrowhead) alongside pyknotic, rounded GC3Ai-positive cells (red arrowhead), showing that there are a mix of morphologically apoptotic NiA and non-apoptotic NiCP cells in the disc proper. See Supplementary Genotypes file for exact genotypes.

Figure 5 – figure supplement 1. (**A**) A *DC*^{NA}*>GC3Ai* control disc driving *UAS-GC3Ai* in the pouch, HA labels all *GC3Ai*-expressing cells, while the cells with activated GC3Ai also have green fluorescence. (**B**) A *DC*^{GluR1}*>>GC3Ai* ablated disc showing GC3Ai-positive NiA cells and, to a lesser extent, GC3Ai-positive WE apoptotic cells. (**C**) A *DC*^{GluR1} *LP>GC3Ai* ablated disc, with HA highlighting the restricted expression of *GC3Ai* to the LP, thus excluding WE cells. (**D-E**) *DC*^{GluR1} ablated discs at 18 hr (**D**) and 36 hr (**E**) with *GC3Ai/TUNEL* double-positive NiA at both time points. (**F-G**) *DC*^{GluR1} ablated discs at 18 hr (**F**) and 36 hr (**G**) showing strong overlap between NiA and yH2Av at 18 hr (arrowheads in **F**) that diminishes by 36 hr (open arrowheads in (**G**). See Supplementary Genotypes file for exact genotypes.

Figure 6 – NiCP have sublethal levels of activated effector caspases. (**A-A'**) A *DC*^{GluR1} *DBS-GFP* ablated disc at 18 hr showing strong overlap between Dcp-1 and *DBS-GFP*-positive NiA/NiCP. (**B-B'''**) *DC*^{GluR1} *CasEx*^{ts}*>G-trace* ablated discs at 18 hr with RFP labeled WE cells, (arrowhead), but no RFP or lineage trage-positive labeling is observed in NiA/NiCP (open arrowheads). (**C**) A *DC*^{hepCA} *CasEx*^{ts}*>G-trace* ablated disc at 18 hr showing a high level of overlap between apoptotic cells and both RFP and the lineage trace (arrowhead). (**D-E**) *DC*^{GluR1} *CasEx>GFP* ablated discs at 18 hr (**D**) and 36 hr (**E**) showing that NiA/NiCP are labeled by *CasExpress* in a sensitized background. See Supplementary Genotypes file for exact genotypes.

Figure 6 – figure supplement 1. (**A**) A *DC*^{GluR1} *CasEx*^{ts}*>G-trace* ablated disc at 36 hr with no lineage-positive NiA/NiCP, despite the presence of clonal patches of cells traced by developmental caspase activity. See Supplementary Genotypes file for exact genotypes.

Figure 7 – Dronc activity in NiCP promotes regeneration. (**A-J**) Representative *DC*^{GluR1} ablated discs at 18 hr (**A**,**C**,**E**,**G** and **I**) with Dcp-1 and Mmp1 labeling, and at 36 hr (**B**,**D**,**F**,**H** and **J**) with EdU labeling, bearing *UAS-y*^{RNAi} (**A-B**), *UAS-mir(RHG)* (**C-D**), *Dronc*^{I29}/+ (**E-F**), *UAS-Dronc*^{DN} (**G-H**), or *UAS-DIAP1* (**I-J**). Open arrowhead in (**F**) indicates a strong reduction in EdU labeling. Open arrowheads in (**I**) show a strong suppression of NiA/NiCP as detected by Dcp-1. (**K**) A quantification of NiA/NiCP number (Dcp-1+ve, Mmp1-ve cells) in *UAS-y*^{RNAi} (n = 11), *UAS-mir(RHG)* (n = 8), *Dronc*^{I29}/+ (n = 10), *UAS- UAS-Dronc*^{DN} (n = 7), and *UAS-DIAP1* (n = 8), ns, not significant, P**** <0.0001. Data were analyzed with a one-way ANOVA followed by a multiple comparisons test. (**L**) A quantification of EdU fluorescence intensity with *UAS-y*^{RNAi} (n = 20), *UAS-mir(RHG)* (n = 14), *Dronc*^{I29}/+ (n = 18) *UAS- UAS-Dronc*^{DN} (n = 17) and *DIAP1* (n = 10), ns, not significant, P*** = 0.0004, P**** <0.0001. Data were analyzed with a one-way ANOVA followed by a multiple comparisons test. (**M**) Regeneration scoring of *DC*^{GluR1} ablated flies in a +/+ versus a *Dronc*^{I29}/+ background. Representative images for regenerated +/+ (left) and *Dronc*^{I29}/+ are shown above the graph. (**N**) A diagram depicting the three different caspase-positive cell types that occur following necrotic ablation. Following necrosis, JNK signaling at the WE promotes Dronc activation, which mediates WE apoptosis and proliferation through the AiP feed forward loop. In the LP, some DAMP-like signal(s) leads to the formation of necrosis-induced apoptosis (NiA), which undergo apoptotic death resulting from high levels of Dronc, Dcp-1 and Drice activity, and necrosis-induced caspase positive (NiCP) cells that utilize Dronc to promote proliferation and subsequent regeneration independent of both JNK and AiP signaling. Both WE apoptosis and NiCP act to promote regeneration through independent mechanisms of Dronc-mediated regenerative proliferation. See Supplementary Genotypes file for exact genotypes.

Figure 7 – figure supplement 1. (**A**) A quantification of regenerated wing size in an unablated control (*DC*^{NA}) wildtype (+/+, males = 17, females = 11) and *Dronc*^{I29}/+ (males = 11, females = 22) background, and following *DC*^{GluR1} ablation in a +/+ (n = 16 males, n = 19 females) and *Dronc*^{I29}/+ (n = 19 males, n = 28 females) background, ns = not significant, P*** = 0.0001, data were analyzed with a one-way ANOVA followed by a multiple comparisons test. See Supplementary Genotypes file for exact genotypes. Representative images for regenerated +/+ (top) and *Dronc*^{I29}/+ (bottom) wings are shown to the right of the graph. See Supplementary Genotypes file for exact genotypes.

Figure 1

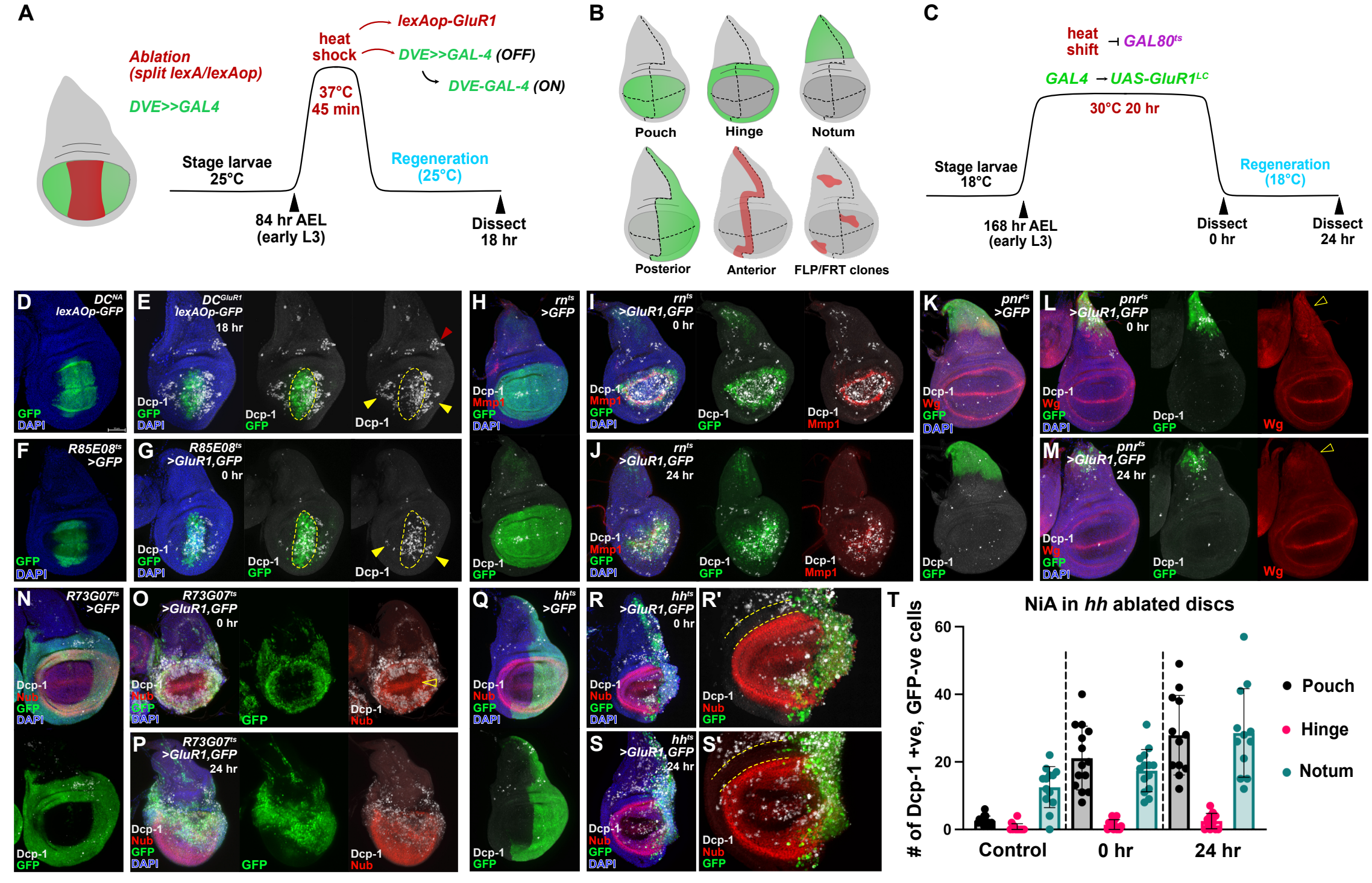
A
Ablation
(split lexA/lexAop)
DVE>>GAL4
heat
shock
lexAop-GluR1
DVE>>GAL-4 (OFF)
DVE-GAL-4 (ON)
37°C
45 min
Stage larvae
25°C
Regeneration
(25°C)
84 hr AEL
(early L3)
Dissect
18 hr
B
Pouch
Hinge
Notum
Posterior
Anterior
FLP/FRT clones
C
heat
shift
GAL80ts
GAL4 → UAS-GluR1LC
30°C 20 hr
Stage larvae
18°C
Regeneration
(18°C)
168 hr AEL
(early L3)
Dissect
0 hr
Dissect
24 hr
D DCNA lexAOp-GFP
E DCGluR1 lexAOp-GFP 18 hr
F R85E08ts >GFP
G R85E08ts >GluR1,GFP 0 hr
H rnts >GFP
I rnts >GluR1,GFP 0 hr
J rnts >GluR1,GFP 24 hr
K pnrts >GFP
L pnrts >GluR1,GFP 0 hr
M pnrts >GluR1,GFP 24 hr
N R73G07ts >GFP
O R73G07ts >GluR1,GFP 0 hr
P R73G07ts >GluR1,GFP 24 hr
Q hhts >GFP
R hhts >GluR1,GFP 0 hr
R'
S hhts >GluR1,GFP 24 hr
S'
Dcp-1
GFP
DAPI
Mmp1
Wg
Nub
T
NiA in hh ablated discs
# of Dcp-1 +ve, GFP-ve cells
60
40
20
0
Control
0 hr
24 hr
Pouch
Hinge
Notum

Figure 2

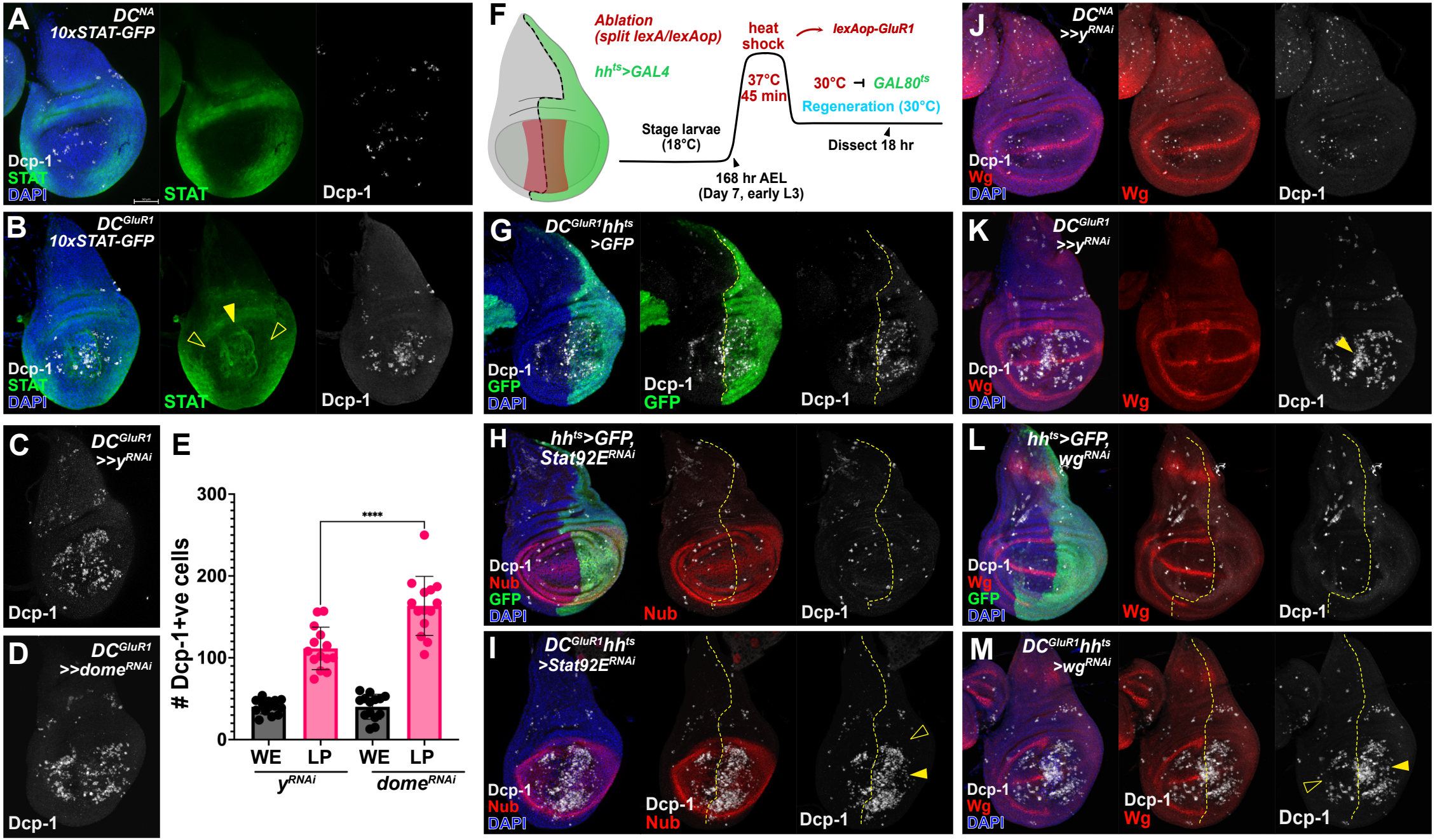
A
DC^NA
10xSTAT-GFP
Dcp-1
STAT
DAPI
STAT
Dcp-1
B
DC^GluR1
10xSTAT-GFP
Dcp-1
STAT
DAPI
STAT
Dcp-1
C
DC^GluR1
>>y^RNAi
Dcp-1
D
DC^GluR1
>>dome^RNAi
Dcp-1
E
Dcp-1+ve cells
300
200
100
0
****
WE
LP
WE
LP
y^RNAi
dome^RNAi
F
Ablation
(split lexA/lexAop)
hh^ts>GAL4
heat
shock
lexAop-GluR1
37°C
45 min
30°C
GAL80^ts
Regeneration (30°C)
Stage larvae
(18°C)
Dissect 18 hr
168 hr AEL
(Day 7, early L3)
G
DC^GluR1 hh^ts
>GFP
Dcp-1
GFP
DAPI
Dcp-1
GFP
Dcp-1
H
hh^ts>GFP,
Stat92E^RNAi
Dcp-1
Nub
GFP
DAPI
Nub
Dcp-1
I
DC^GluR1 hh^ts
>Stat92E^RNAi
Dcp-1
Nub
DAPI
Dcp-1
Nub
Dcp-1
J
DC^NA
>>y^RNAi
Dcp-1
Wg
DAPI
Wg
Dcp-1
K
DC^GluR1
>>y^RNAi
Dcp-1
Wg
DAPI
Wg
Dcp-1
L
hh^ts>GFP,
wg^RNAi
Dcp-1
Wg
GFP
DAPI
Wg
Dcp-1
M
DC^GluR1 hh^ts
>wg^RNAi
Dcp-1
Wg
DAPI
Dcp-1
Wg
Dcp-1

Figure 3

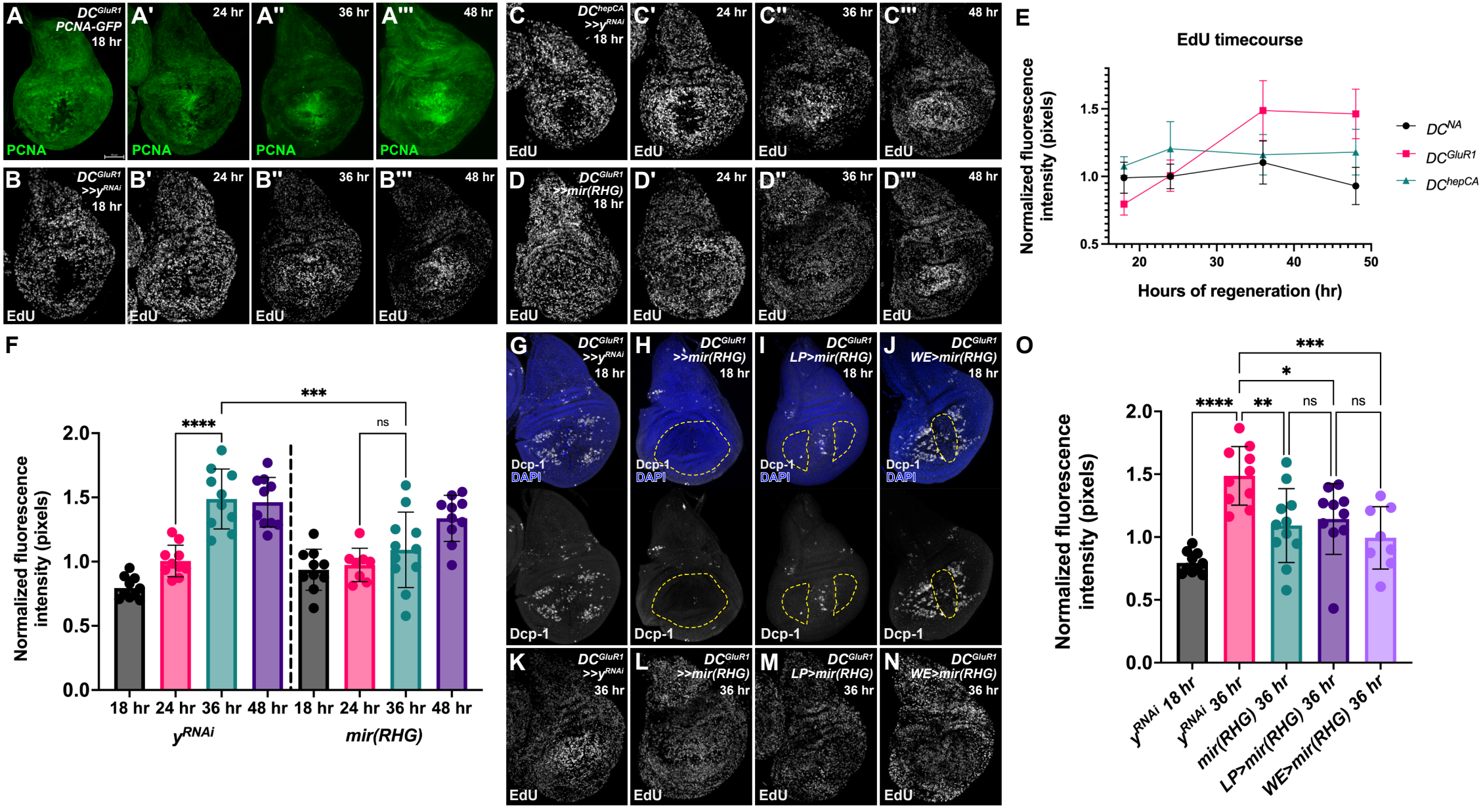
A
DC^GluR1 PCNA-GFP
18 hr
A'
24 hr
A''
36 hr
A'''
48 hr
PCNA
B
DC^GluR1 >>y^RNAi
18 hr
B'
24 hr
B''
36 hr
B'''
48 hr
EdU
C
DC^hepCA >>y^RNAi
18 hr
C'
24 hr
C''
36 hr
C'''
48 hr
D
DC^GluR1 >>mir(RHG)
18 hr
D'
24 hr
D''
36 hr
D'''
48 hr
E
EdU timecourse
Normalized fluorescence intensity (pixels)
Hours of regeneration (hr)
DC^NA
DC^GluR1
DC^hepCA
F
Normalized fluorescence intensity (pixels)
****
***
ns
18 hr 24 hr 36 hr 48 hr 18 hr 24 hr 36 hr 48 hr
y^RNAi
mir(RHG)
G
DC^GluR1 >>y^RNAi
18 hr
H
DC^GluR1 >>mir(RHG)
18 hr
I
DC^GluR1 LP>mir(RHG)
18 hr
J
DC^GluR1 WE>mir(RHG)
18 hr
Dcp-1
DAPI
K
DC^GluR1 >>y^RNAi
36 hr
L
DC^GluR1 >>mir(RHG)
36 hr
M
DC^GluR1 LP>mir(RHG)
36 hr
N
DC^GluR1 WE>mir(RHG)
36 hr
O
Normalized fluorescence intensity (pixels)
****
**
*
***
ns
ns
y^RNAi 18 hr
y^RNAi 36 hr
mir(RHG) 36 hr
LP>mir(RHG) 36 hr
WE>mir(RHG) 36 hr

Figure 4

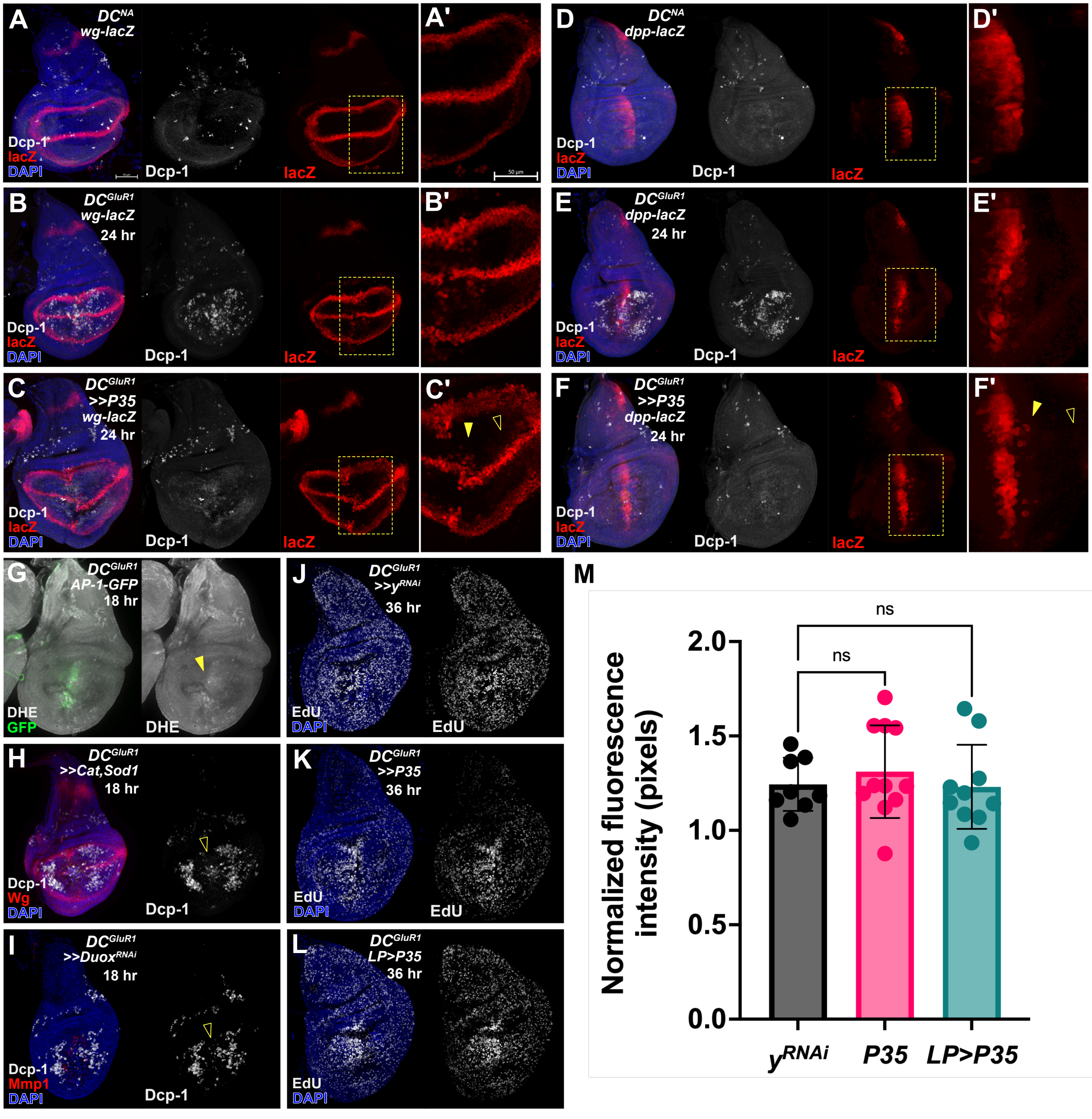
A
DC^NA
wg-lacZ
Dcp-1
lacZ
DAPI
Dcp-1
lacZ
A'
50 µm
B
DC^GluR1
wg-lacZ
24 hr
Dcp-1
lacZ
DAPI
Dcp-1
lacZ
B'
C
DC^GluR1
>>P35
wg-lacZ
24 hr
Dcp-1
lacZ
DAPI
Dcp-1
lacZ
C'
D
DC^NA
dpp-lacZ
Dcp-1
lacZ
DAPI
Dcp-1
lacZ
D'
E
DC^GluR1
dpp-lacZ
24 hr
Dcp-1
lacZ
DAPI
Dcp-1
lacZ
E'
F
DC^GluR1
>>P35
dpp-lacZ
24 hr
Dcp-1
lacZ
DAPI
Dcp-1
lacZ
F'
G
DC^GluR1
AP-1-GFP
18 hr
DHE
GFP
DHE
J
DC^GluR1
>>y^RNAi
36 hr
EdU
DAPI
EdU
H
DC^GluR1
>>Cat,Sod1
18 hr
Dcp-1
Wg
DAPI
Dcp-1
K
DC^GluR1
>>P35
36 hr
EdU
DAPI
EdU
I
DC^GluR1
>>Duox^RNAi
18 hr
Dcp-1
Mmp1
DAPI
Dcp-1
L
DC^GluR1
LP>P35
36 hr
EdU
DAPI
M
Normalized fluorescence intensity (pixels)
2.0
1.5
1.0
0.5
0.0
ns
ns
y^RNAi
P35
LP>P35

Figure 5

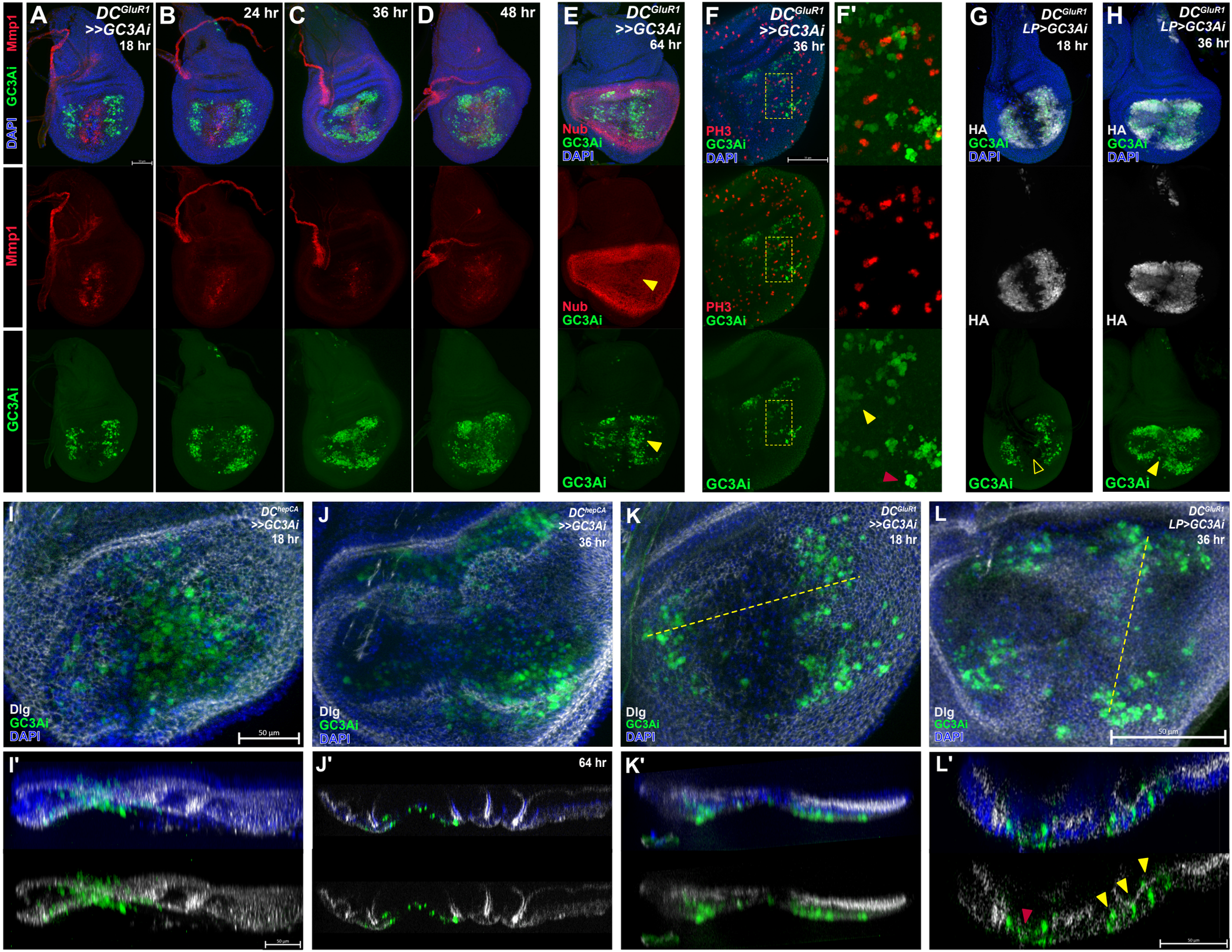
A
DC^GluR1 >>GC3Ai
18 hr
B
24 hr
C
36 hr
D
48 hr
E
DC^GluR1 >>GC3Ai
64 hr
F
DC^GluR1 >>GC3Ai
36 hr
F'
G
DC^GluR1 LP>GC3Ai
18 hr
H
DC^GluR1 LP>GC3Ai
36 hr
Mmp1
GC3Ai
DAPI
Nub
PH3
HA
I
DC^hepCA >>GC3Ai
18 hr
J
DC^hepCA >>GC3Ai
36 hr
K
DC^GluR1 >>GC3Ai
18 hr
L
DC^GluR1 LP>GC3Ai
36 hr
Dlg
50 µm
I'
J'
64 hr
K'
L'

Figure 6

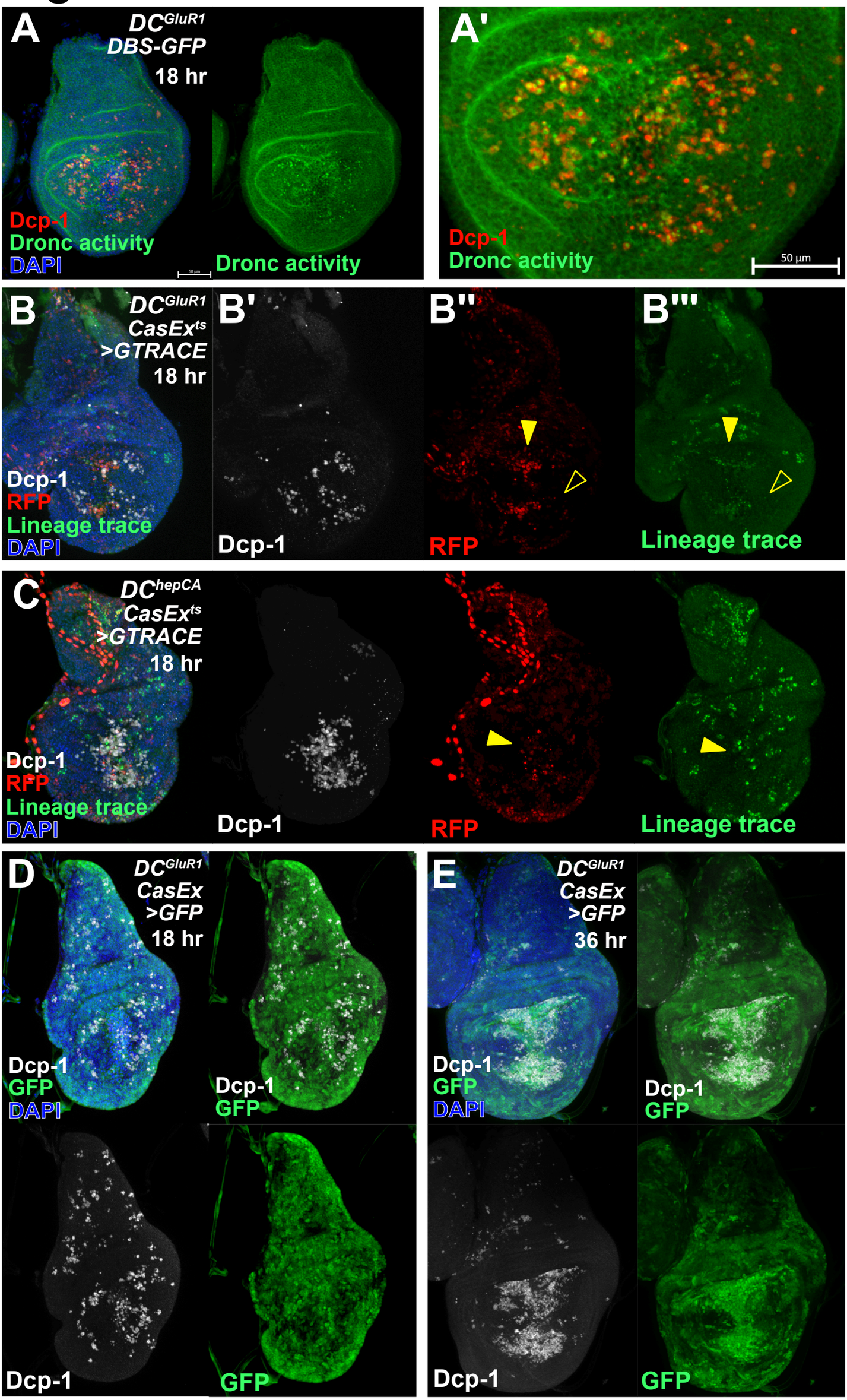
A
DC^GluR1
DBS-GFP
18 hr
Dcp-1
Dronc activity
DAPI
Dronc activity
A'
Dcp-1
Dronc activity
50 µm
B
DC^GluR1
CasEx^ts
>GTRACE
18 hr
Dcp-1
RFP
Lineage trace
DAPI
B'
Dcp-1
B''
RFP
B'''
Lineage trace
C
DC^hepCA
CasEx^ts
>GTRACE
18 hr
Dcp-1
RFP
Lineage trace
DAPI
Dcp-1
RFP
Lineage trace
D
DC^GluR1
CasEx
>GFP
18 hr
Dcp-1
GFP
DAPI
Dcp-1
GFP
Dcp-1
GFP
E
DC^GluR1
CasEx
>GFP
36 hr
Dcp-1
GFP
DAPI
Dcp-1
GFP
Dcp-1
GFP

Figure 7

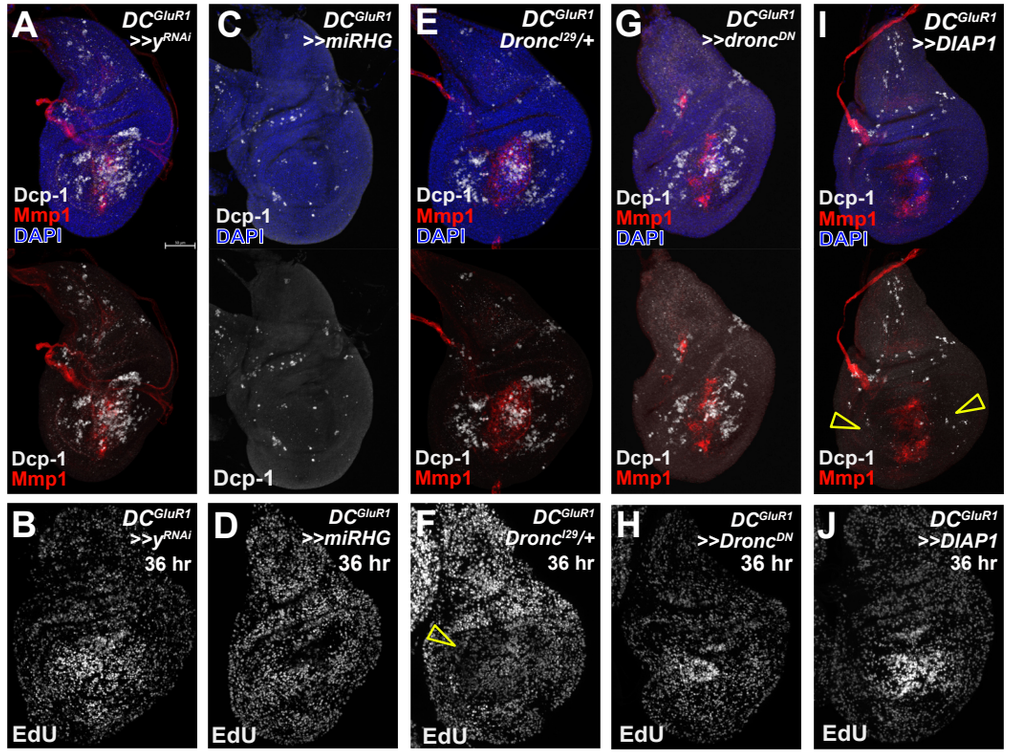
A
DC^GluR1 >>y^RNAi
Dcp-1
Mmp1
DAPI
Dcp-1
Mmp1
B
DC^GluR1 >>y^RNAi
36 hr
EdU
C
DC^GluR1 >>miRHG
Dcp-1
DAPI
Dcp-1
D
DC^GluR1 >>miRHG
36 hr
EdU
E
DC^GluR1 Dronc^I29/+
Dcp-1
Mmp1
DAPI
Dcp-1
Mmp1
F
DC^GluR1 Dronc^I29/+
36 hr
EdU
G
DC^GluR1 >>dronc^DN
Dcp-1
Mmp1
DAPI
Dcp-1
Mmp1
H
DC^GluR1 >>Dronc^DN
36 hr
EdU
I
DC^GluR1 >>DIAP1
Dcp-1
Mmp1
DAPI
Dcp-1
Mmp1
J
DC^GluR1 >>DIAP1
36 hr
EdU

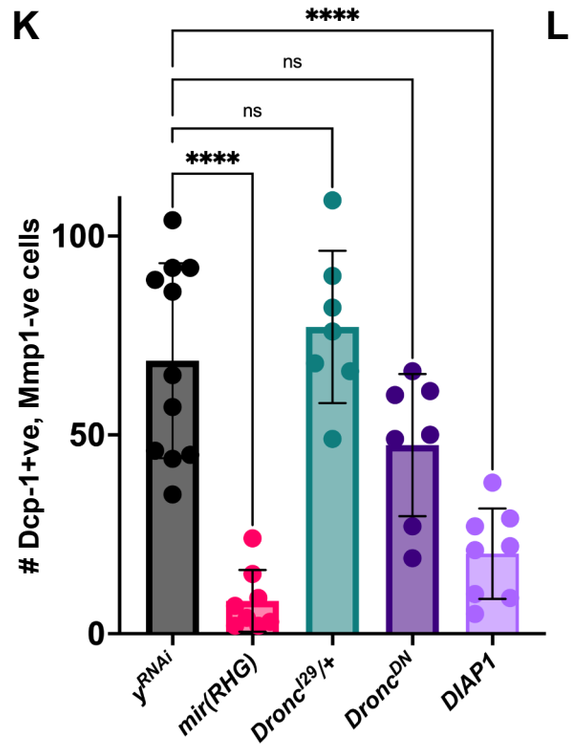
K
Dcp-1+ve, Mmp1-ve cells
100
50
0
****
ns
ns
****
y^RNAi
mir(RHG)
Dronc^I29/+
Dronc^DN
DIAP1

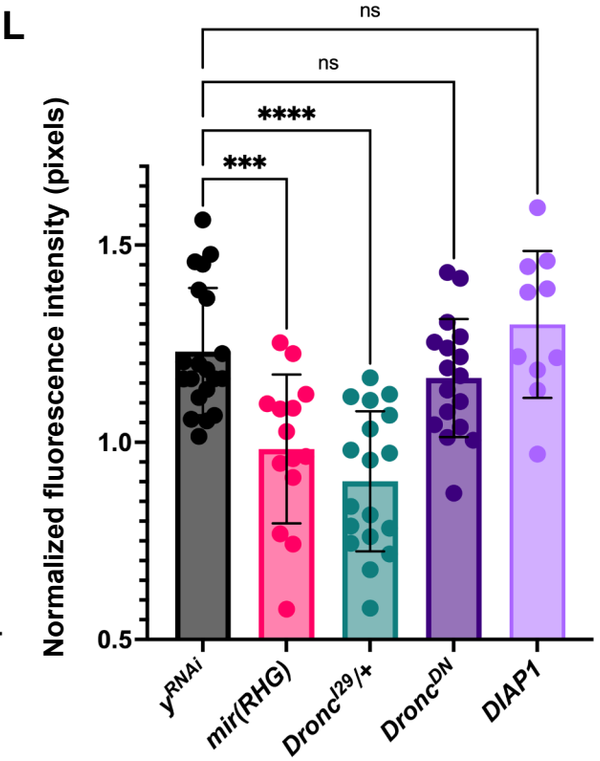
L
Normalized fluorescence intensity (pixels)
1.5
1.0
0.5
ns
ns
****
***
y^RNAi
mir(RHG)
Dronc^I29/+
Dronc^DN
DIAP1

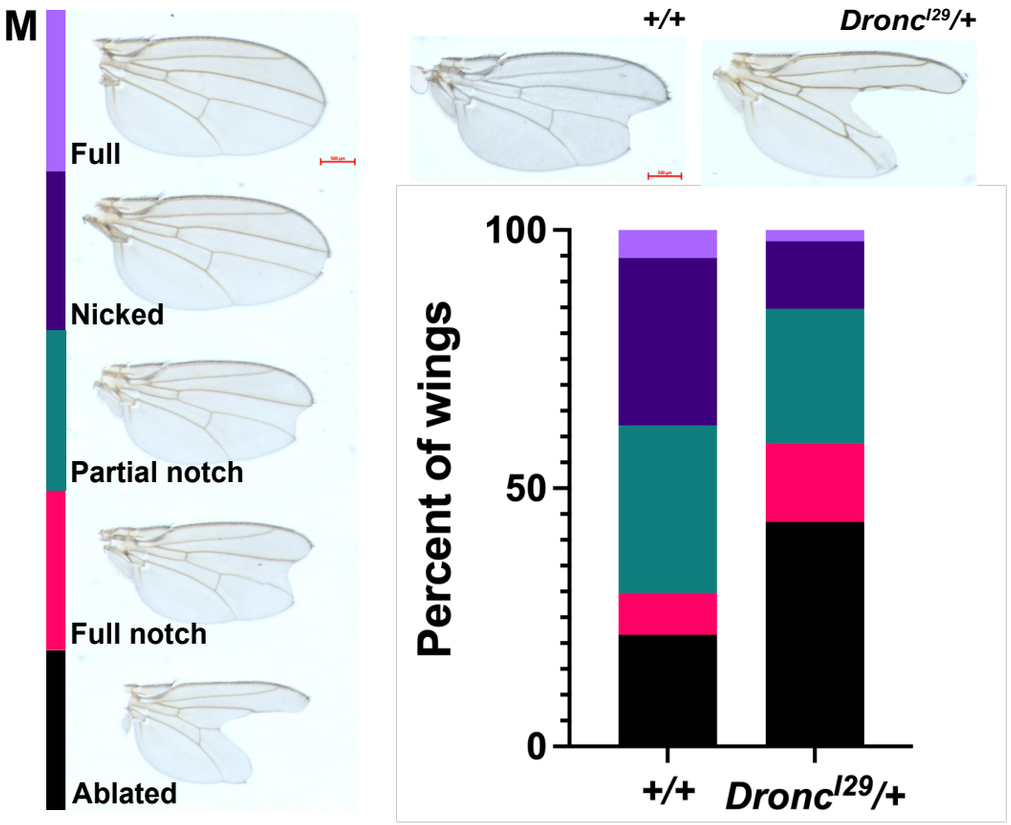
M
Full
Nicked
Partial notch
Full notch
Ablated
+/+
Dronc^I29/+
Percent of wings
100
50
0
+/+
Dronc^I29/+

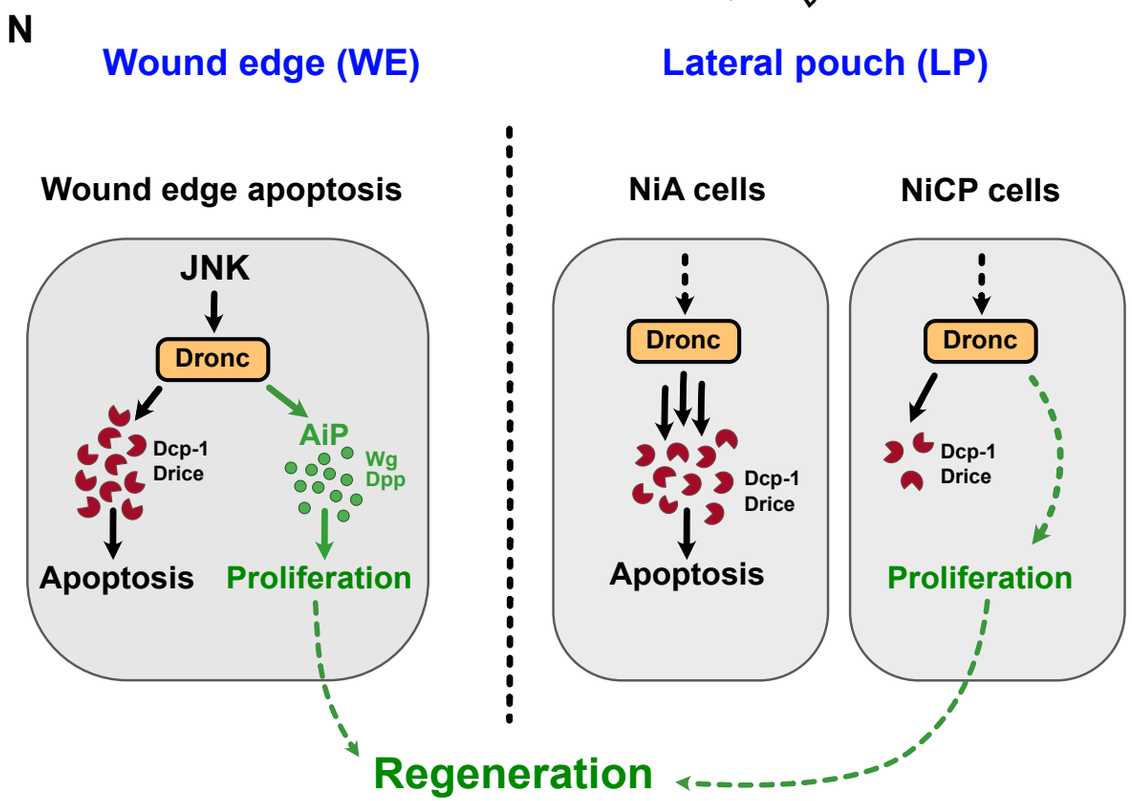
N
Wound edge (WE)
Lateral pouch (LP)
Wound edge apoptosis
JNK
Dronc
Dcp-1
Drice
AiP
Wg
Dpp
Apoptosis
Proliferation
NiA cells
Dronc
Dcp-1
Drice
Apoptosis
NiCP cells
Dronc
Dcp-1
Drice
Proliferation
Regeneration

Figure S1

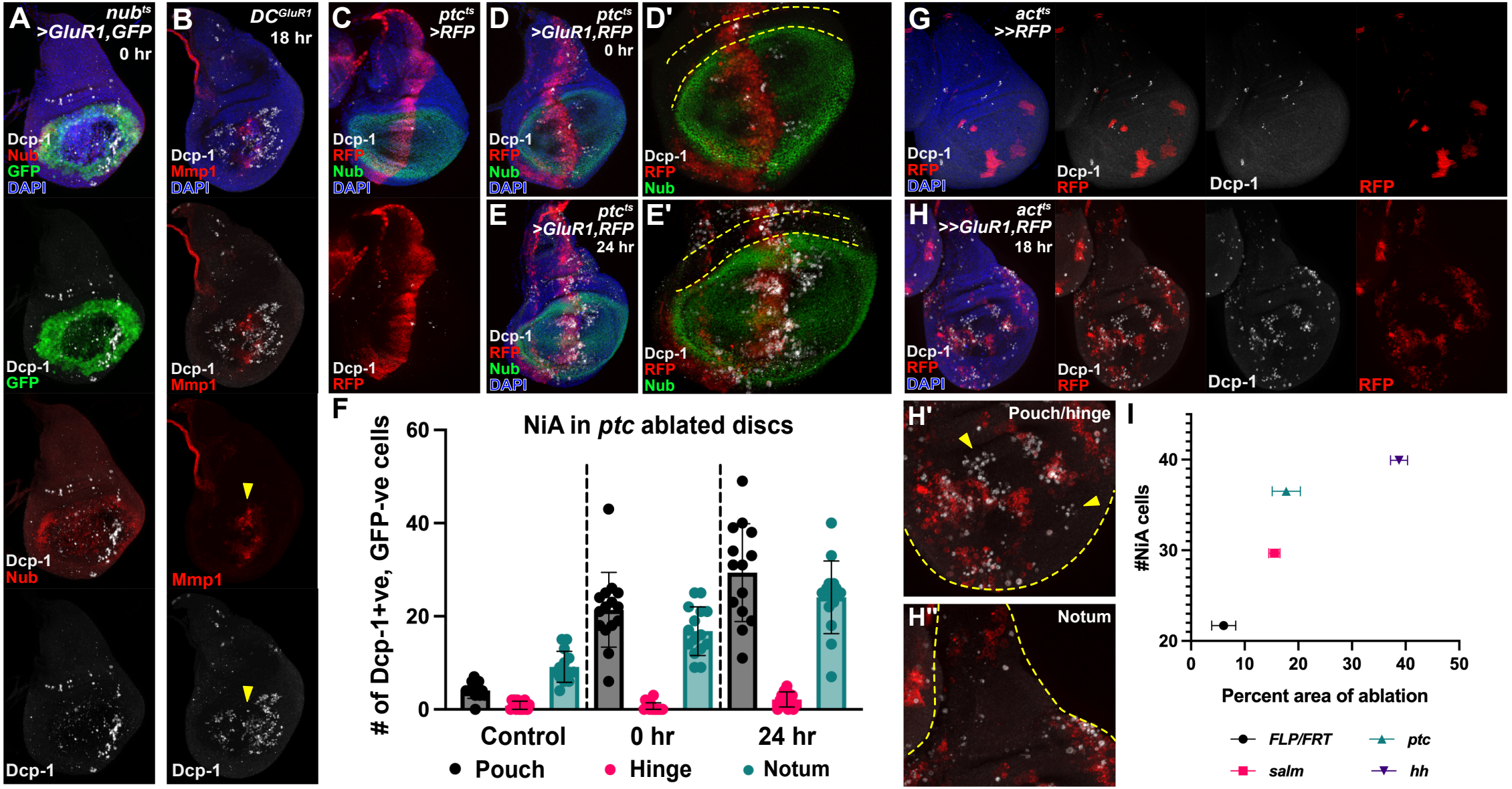
A
nubts >GluR1,GFP
0 hr
Dcp-1
Nub
GFP
DAPI
B
DCGluR1
18 hr
Dcp-1
Mmp1
DAPI
C
ptcts >RFP
Dcp-1
RFP
Nub
DAPI
D
ptcts >GluR1,RFP
0 hr
D'
E
ptcts >GluR1,RFP
24 hr
E'
G
actts >>RFP
H
actts >>GluR1,RFP
18 hr
F
NiA in ptc ablated discs
# of Dcp-1+ve, GFP-ve cells
Control
0 hr
24 hr
Pouch
Hinge
Notum
H'
Pouch/hinge
H''
Notum
I
#NiA cells
Percent area of ablation
FLP/FRT
ptc
salm
hh

Figure S2

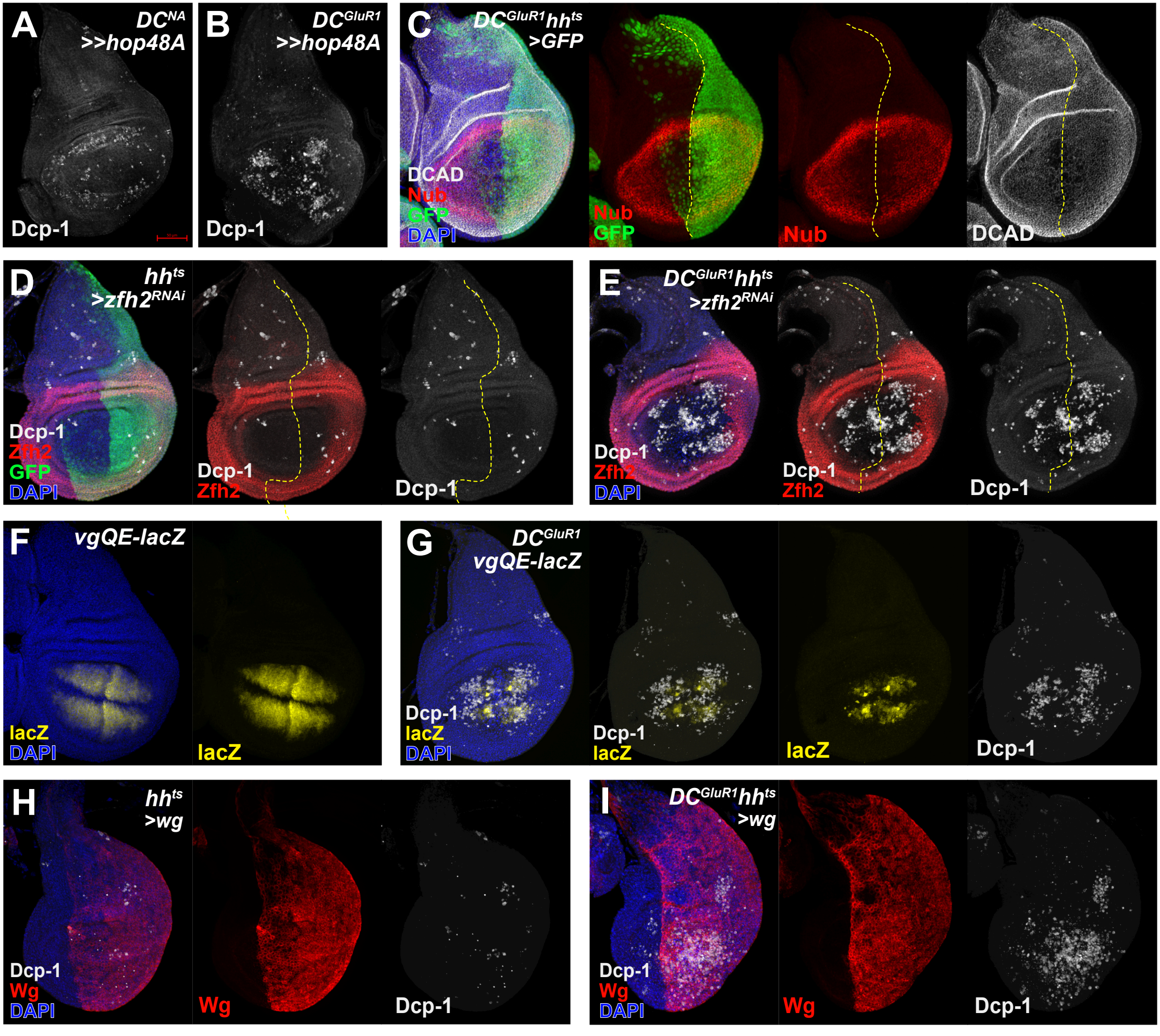
A
DC^NA >>hop48A
Dcp-1
B
DC^GluR1 >>hop48A
Dcp-1
C
DC^GluR1 hh^ts >GFP
DCAD
Nub
GFP
DAPI
Nub
GFP
Nub
DCAD
D
hh^ts >zfh2^RNAi
Dcp-1
Zfh2
GFP
DAPI
Dcp-1
Zfh2
Dcp-1
E
DC^GluR1 hh^ts >zfh2^RNAi
Dcp-1
Zfh2
DAPI
Dcp-1
Zfh2
Dcp-1
F
vgQE-lacZ
lacZ
DAPI
lacZ
G
DC^GluR1 vgQE-lacZ
Dcp-1
lacZ
DAPI
Dcp-1
lacZ
lacZ
Dcp-1
H
hh^ts >wg
Dcp-1
Wg
DAPI
Wg
Dcp-1
I
DC^GluR1 hh^ts >wg
Dcp-1
Wg
DAPI
Wg
Dcp-1

Figure S3

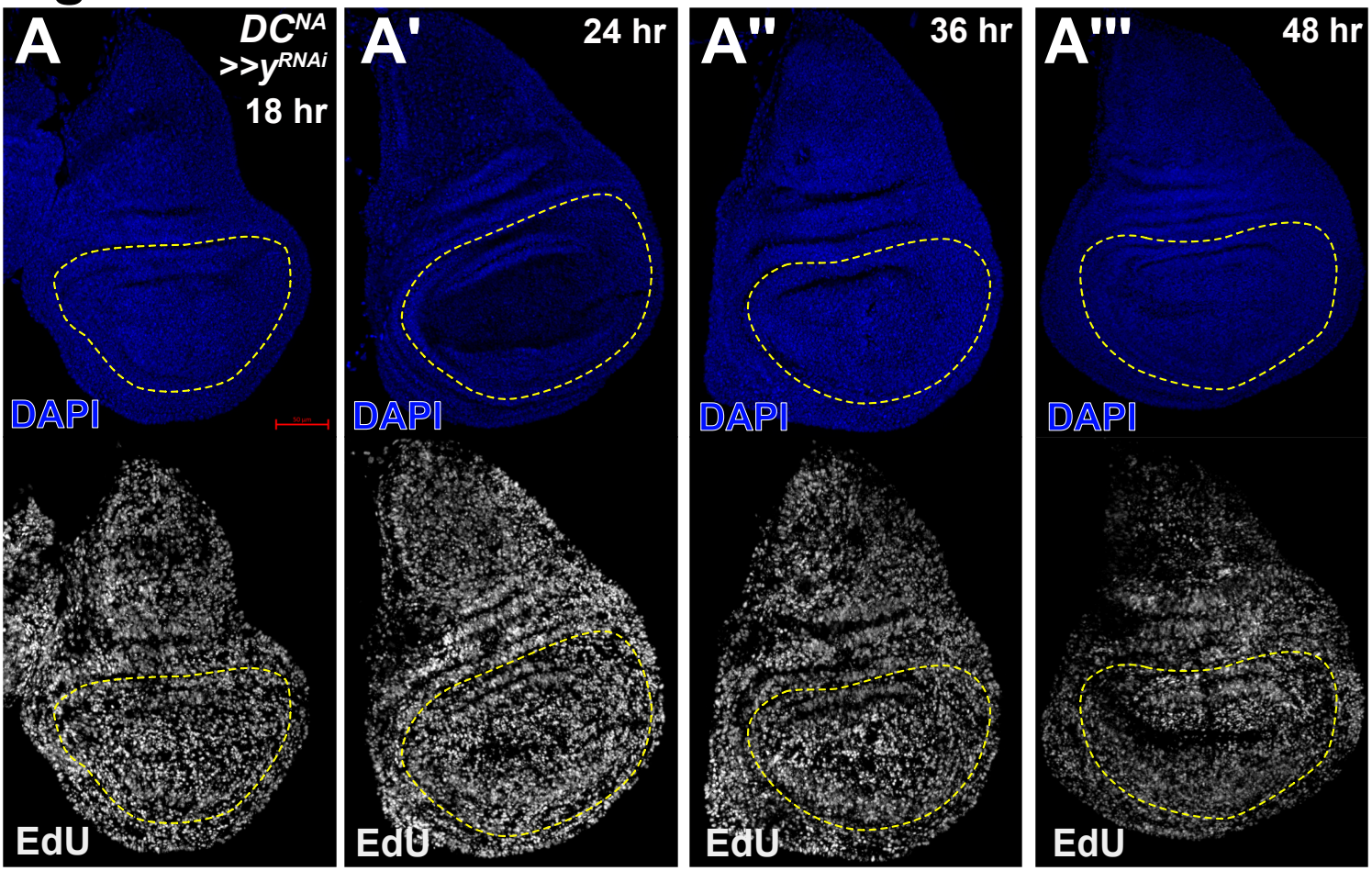
A
DC^NA >>y^RNAi
18 hr
DAPI
EdU
A'
24 hr
DAPI
EdU
A''
36 hr
DAPI
EdU
A'''
48 hr
DAPI
EdU

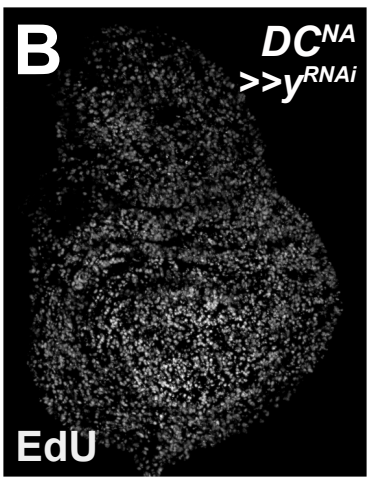
B
DC^NA >>y^RNAi
EdU

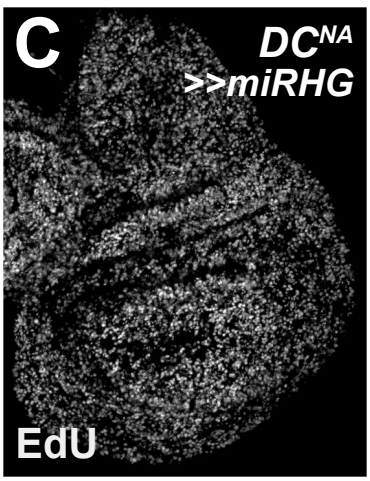
C
DC^NA >>miRHG
EdU

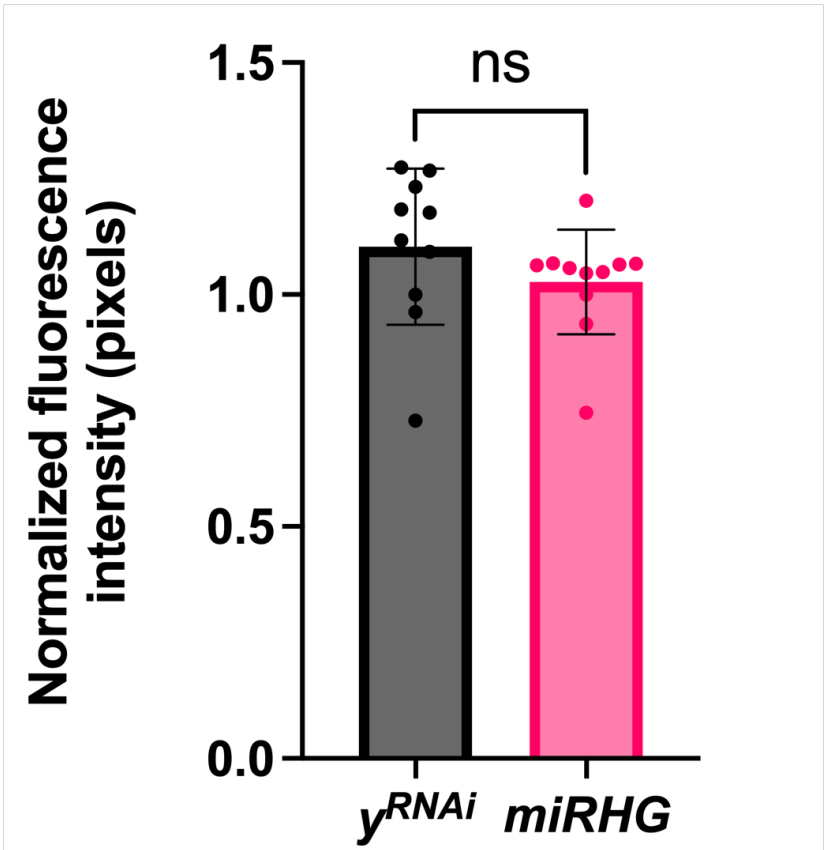
D
Normalized fluorescence intensity (pixels)
1.5
1.0
0.5
0.0
ns
y^RNAi
miRHG

Figure S4

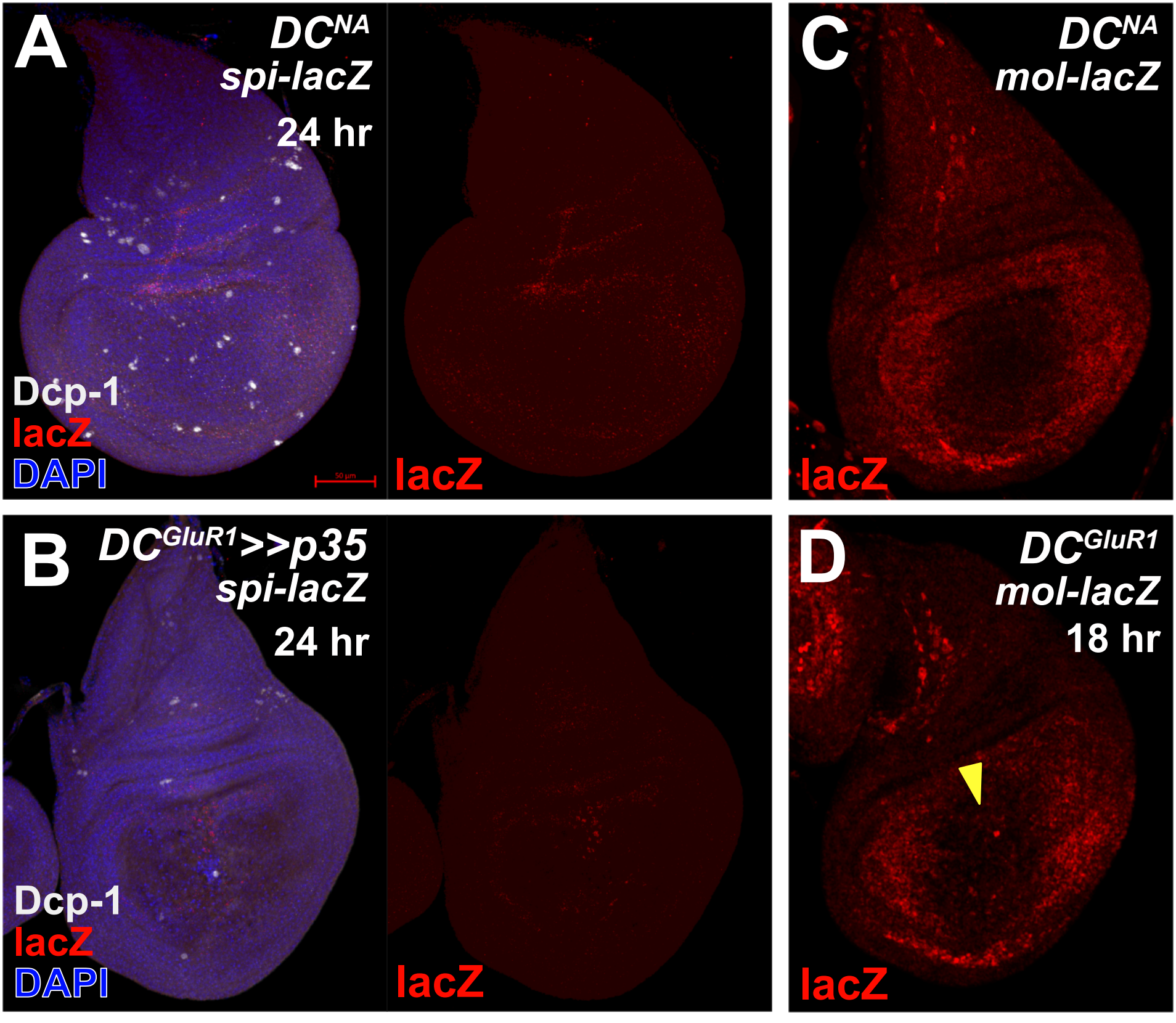
A
DC^NA
spi-lacZ
24 hr
Dcp-1
lacZ
DAPI
50 µm
lacZ
C
DC^NA
mol-lacZ
lacZ
B
DC^GluR1>>p35
spi-lacZ
24 hr
Dcp-1
lacZ
DAPI
lacZ
D
DC^GluR1
mol-lacZ
18 hr
lacZ

Figure S5

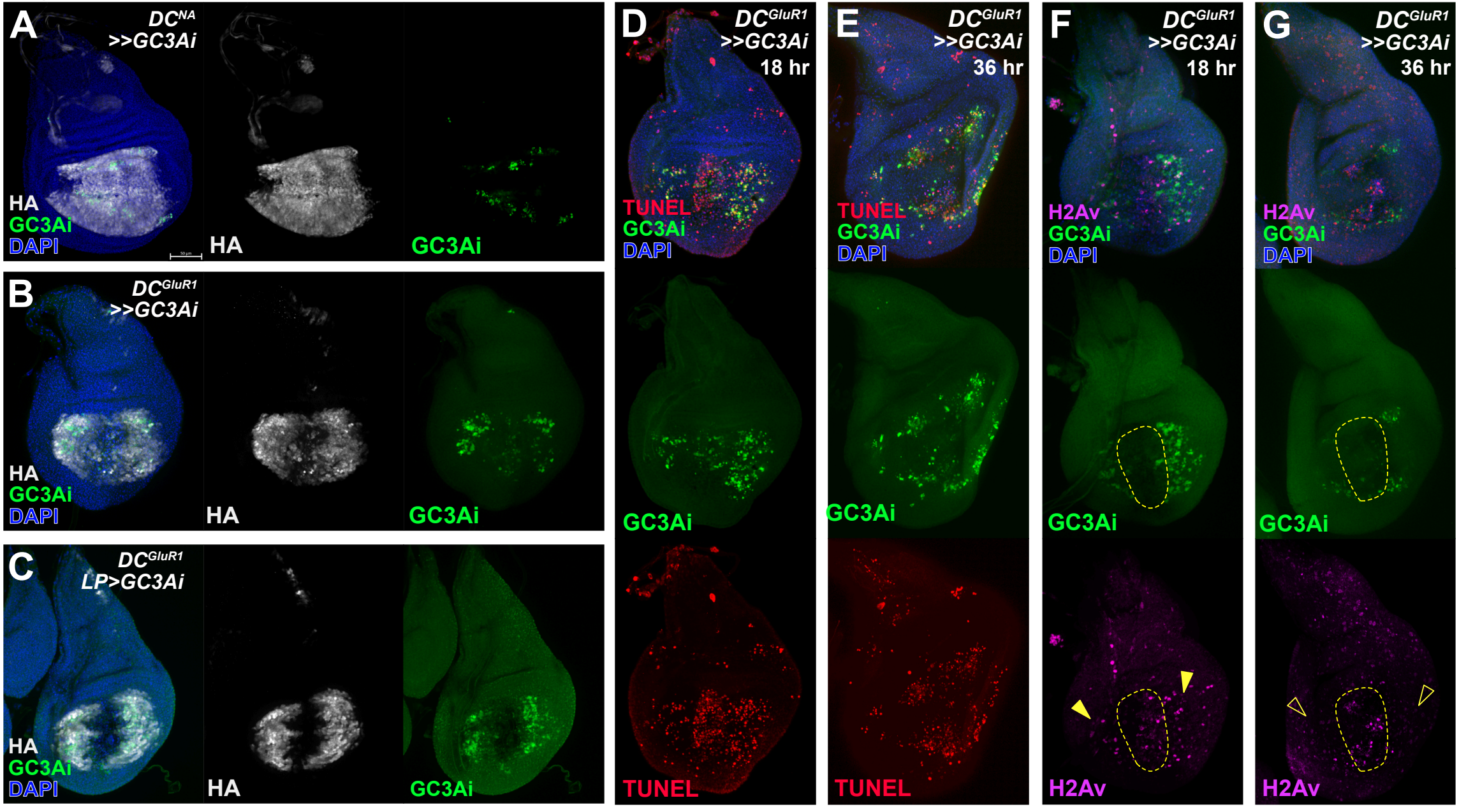
A
DC^NA >>GC3Ai
HA
GC3Ai
DAPI
HA
GC3Ai
B
DC^GluR1 >>GC3Ai
HA
GC3Ai
DAPI
HA
GC3Ai
C
DC^GluR1 LP>GC3Ai
HA
GC3Ai
DAPI
HA
GC3Ai
D
DC^GluR1 >>GC3Ai
18 hr
TUNEL
GC3Ai
DAPI
GC3Ai
TUNEL
E
DC^GluR1 >>GC3Ai
36 hr
TUNEL
GC3Ai
DAPI
GC3Ai
TUNEL
F
DC^GluR1 >>GC3Ai
18 hr
H2Av
GC3Ai
DAPI
GC3Ai
H2Av
G
DC^GluR1 >>GC3Ai
36 hr
H2Av
GC3Ai
DAPI
GC3Ai
H2Av

Figure S6

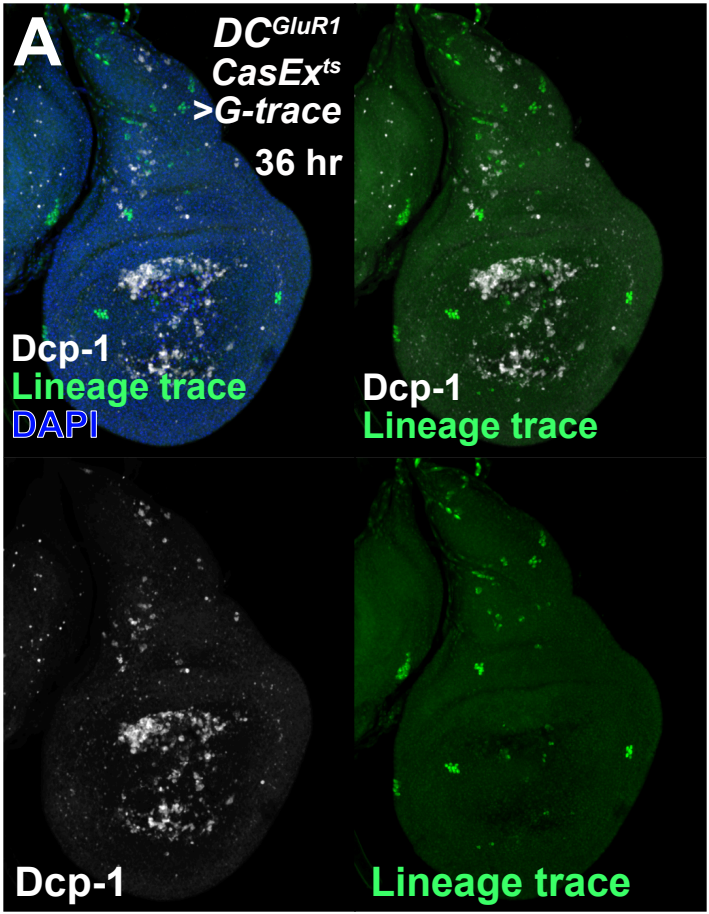
A
DC^GluR1
CasEx^ts
>G-trace
36 hr
Dcp-1
Lineage trace
DAPI
Dcp-1
Lineage trace
Dcp-1
Lineage trace

Figure S7

A

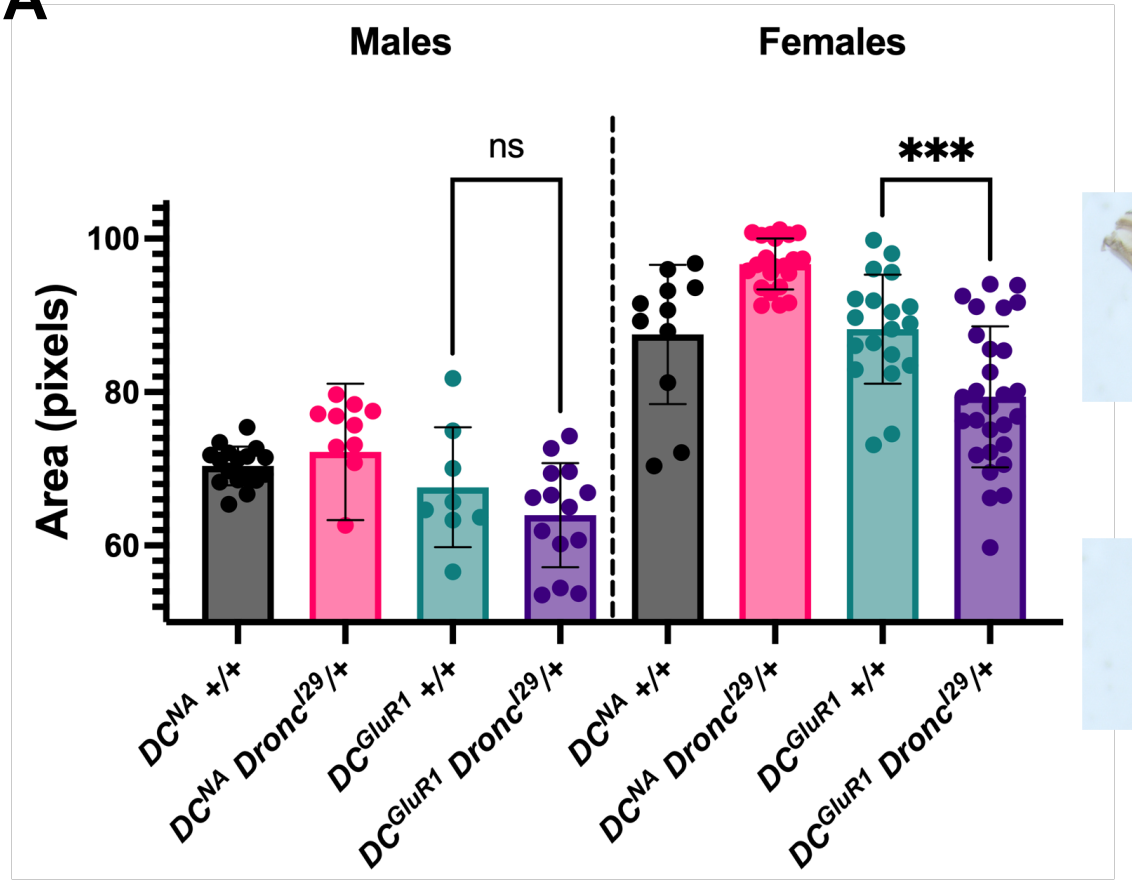
Males
Females
ns
***
Area (pixels)
100
80
60
DC^NA +/+
DC^NA Dronc^I29/+
DC^GluR1 +/+
DC^GluR1 Dronc^I29/+
DC^NA +/+
DC^NA Dronc^I29/+
DC^GluR1 +/+
DC^GluR1 Dronc^I29/+

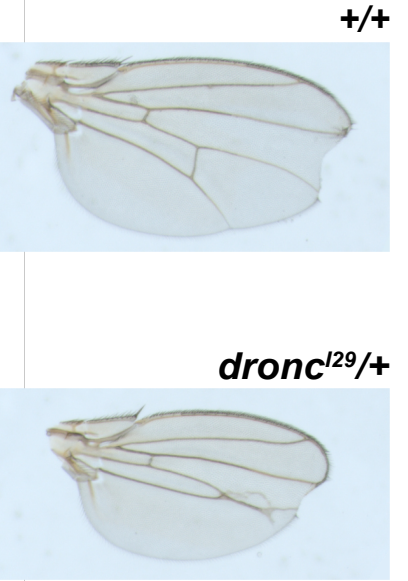
+/+
dronc^I29/+